Dissertation

submitted to the

Combined Faculties for the Natural Sciences and for Mathematics

of the Ruperto-Carola University of Heidelberg, Germany

for the degree of

Doctor of Natural Sciences

presented by

M.Sc. Noam Pilpel
born in Jerusalem, Israel

Dissertation

submitted to the

Combined Faculties for the Natural Sciences and for Mathematics

of the Ruperto-Carola University of Heidelberg, Germany

for the degree of

Doctor of Natural Sciences

presented by

M.Sc. Noam Pilpel
born in Jerusalem, Israel
Oral-examination: March 27th, 2009

Biochemical and Functional Analysis of γ-Protocadherin Intracellular Signaling Pathways

Referees: Prof. Dr. Peter H. Seeburg
Priv.-Doz. Dr. Matthias Klugmann

Erklärung gemäß § 8 (3) b) und c) der Promotionsordnung:

Ich erkläre hiermit, daß ich die vorgelegte Dissertation selbst verfaßt und mich dabei keiner anderen als der von mir ausdrücklich bezeichneten Quellen und Hilfen bedient habe. Desweiteren erkläre ich hiermit, daß ich an keiner anderen Stelle ein Prüfungsverfahren beantragt bzw. die Dissertation in dieser oder anderer Form bereits anderweitig als Prüfungsarbeit verwendet oder einer anderen Fakultät als Dissertation vorgelegt habe.

Heidelberg, den 27 Januar 2009

For Eden and Yair

Summary

The precisely organized complexity of the central nervous system (CNS) requires an enormous number of specific cell-cell interactions, presumably mediated by a diverse array of membrane associated proteins. The classic cadherins are known to play essential roles in the maintenance of neuronal connectivity and synaptic plasticity. Three complex genomic loci encoding proteins of the cadherin superfamily, the α-, β-, and γ- clustered protocadherins (Pcdhs), have been hypothesized to take part in this task. Their large number, diverse expression pattern during neurogenesis, and partial synaptic localization suggest a role in synaptogenesis. The genomic architecture of the clustered Pcdhs is reminiscent of the immunoglobulin and T-cell receptor clusters which confer the huge variety of antibody molecules: within each cluster, exons encoding variable extracellular and transmembrane domains are alternatively spliced onto a cluster-specific conserved intracellular domain. Thus, Pcdhs confer molecular diversity on the cell surface, with conserved signaling mechanisms in the cytoplasm.

However, the physiological role of Pcdhs as well as the reason for the diversity of extracellular domains and the conservation of the intracellular domain have remained elusive. Our goal was the elucidation of the signal transduction pathways downstream of γ-Pcdh. To this end, we attempted to identify proteins that interact with the conserved intracellular domain of γ-Pcdhs (γ-ICD). We purified specific polyclonal antibodies targeted against the γ-ICD, and used them to immunoprecipitate interacting proteins from mouse forebrain lysates. Mass spectrometry analysis and subsequent co-immunoprecipitation identified novel proteins involved in signal transduction pathways related to cell cycle control, synaptic plasticity and memory formation. To study the role of γ-Pcdh intracellular signaling *in vivo*, we additionally established a viral gene-delivery system into neonatal (P0) mouse brains. This method enabled us to efficiently overexpress the γ-ICD, which allowed us to study the intracellular signaling of γ-Pcdhs. Using this system we uncovered novel physiological effects of γ-ICD overexpression in inhibitory synapses of the cortex, with possible implications for synaptic transmission and plasticity.

Zusammenfassung

Für die exakten Verschaltungen im zentralen Nervensystem, die wahrscheinlich durch unterschiedlichste membranassoziierte Proteine bestimmt werden, sind sehr viele spezifische Zellinteraktionen notwendig. Klassische Cadherine sind dabei nicht nur für die Integrität der neuronalen Vernetzung, sondern auch für synaptische Plastizität essenziell. Eine Unterklasse der Cadherine, die auf drei komplexen genomischen Loci geclusterten α-, β-, und γ-Protocadherine, sind wahrscheinlich auch daran beteiligt. Insbesondere ihre hohe Anzahl, ihr unterschiedliches Expressionsmuster während der Neurogenese und ihre synaptische Verankerung legen die Vermutung auf wichtige Funktionen während der Synaptogenese nahe. Die genomische Anordnung dieser geclusterten Protocadherine erinnert strukturell stark an Immunglobulin und T-Zell Rezeptor Gen-Cluster, welche für die enorme Vielfalt von Antikörpervarianten verantwortlich sind. Dabei werden unterschiedliche Cluster-spezifische Exone, welche die Extrazelluläre- und Transmembrandomäne kodieren, an Exone für eine einheitliche intrazelluläre Domäne gespleisst. Geclusterte Protocadherine vernetzen daher die molekulare Vielfalt an der Zelloberfläche mit einheitlichen zytoplasmatischen Signalwegen. Leider sind bis heute weder physiologische Relevanz noch Grund dieser extrazellulären Vielfalt in Verbindung mit einheitlichen intrazellulären Signalwegen bekannt. Ziel der vorliegenden Arbeit war die Beschreibung intrazellulärer Signalwege von γ-Protocadherinen. Zuerst identifizierten wir Proteine, welche an die γ-Protocadherin spezifische intrazelluläre Domäne (γ-ICD) binden. Dazu reinigten wir polyklonale Antikörper gegen die γ-ICD und immunpräzipitierten damit Bindungspartner aus Maushirnlysaten. Mit Hilfe von massenspektrometrischen Analysen, gefolgt von Co-Immunpräzipitationen, konnten wir neue Interaktionspartner mit bereits bekannten Funktionen während synaptischer Plastizität finden. Um intrazelluläre Signalwege von γ-Protocadherinen und deren Interaktionspartnern *in vivo* besser zu verstehen, etablierten wir eine Methode zum Virus-vermittelten Gentransfer in neugeborene Mäuse. Diese Methode ermöglichte die Überexpression der γ-ICD, sowie die erste elektrophysiologische Beschreibung γ-Protocadherin induzierter Effekte an inhibitorischen Synapsen im Kortex.

1. Introduction

The human brain is the most complex structure known to us, with about 10^{12} neurons, forming 10^{15} connections (Kandel et al., 2000).

In comparison to these staggering numbers, the amount of genetic information encoded by our DNA is surprisingly small. Several biological mechanisms allow to establish this intricate brain circuitry. These include combinatorial use of multiple guidance cues, and the refinement of connections based on the correlated firing activity of neurons. Epigenetic modifications also contribute to phenotypic hard-wiring at the cellular level (Schmucker and Flanagan, 2004; Sweatt, 2009).

When searching for the main constituents contributing, at least partially, to the establishment of the overwhelming specific wiring of the brain, attention is drawn to the large superfamily of the cadherins (Kohmura et al., 1998), and within this family, to clustered Protocadherins (Pcdhs) (Lefebvre et al., 2008).

In the following section I will detail several properties supporting the role of cadherins, and more specifically, γ-Protocadherins (γ-Pcdhs), in forming the basic wiring diagram of the brain.

1.1 The cadherin superfamily

The cadherin superfamily of proteins includes more than 100 members, almost all of which are transmembrane proteins. In general, cadherins are glycoproteins which function in calcium-dependent, selective cell-cell interactions (Wu and Maniatis, 1999, and references therein: Takeichi, 1991, 1995; Marrs and Nelson, 1996). The cadherins contain extracellular cadherin ectodomains (ECs) in different numbers, a single transmembrane and a cytoplasmic domain (Takeichi, 1990; Uemura, 1998). Classic cadherins display a homophilic binding interface embedded within the first (N-terminal) EC1 domain (Morishita and Yagi, 2007).

Cadherins can be further divided into several sub-families: the classic cadherins, desmosomal cadherins, protocadherins, Flamingo/CELSRs and FAT, serving different biological functions (Tepass et al., 2000; Redies et al., 2005). Classic and desmosomal

cadherins, for example, are cell adhesion proteins, but most other sub-families do not display strong adhesion properties, and are therefore probably more important for signal transduction (Takeichi, 2007). Indeed, cell adhesion and signal transduction are closely linked, as classic signal transduction molecules such as Notch-delta, neuroligin-neurexin, and Eph-ephrin, can also promote cell adhesion (Nguyen and Sudhof, 1997; Ahimou et al., 2004; Sela-Donenfeld and Wilkinson, 2005).

1.2 Protocadherins

Protocadherins (Pcdhs) are the largest family of proteins within the cadherin superfamily. More than 70 different Pcdh genes have been identified (Morishita and Yagi, 2007). The term Pcdhs was coined after the way these proteins were identified, by PCR with degenerate primers, targeted against cadherin ectodomains. Pcdhs were isolated from a wide range of vertebrates and invertebrates, which suggested an early primordial cadherin motif, a "proto" cadherin (Sano et al., 1993).

The Pcdh family includes clustered and non-clustered Pcdhs (Redies et al., 2005). Clustered Pcdhs comprise the larger family, with over 50 identified members. Three families of clustered Pcdhs have been identified: the α, β and γ Pcdhs (designated α-, β- and γ-Pcdhs). The genes for these proteins are arrayed in tandem on a single chromosome (human chromosome 5 and mouse chromosome 18 (Wu and Maniatis, 1999). The overall genomic organization of Pcdhs is conserved in all vertebrates, however, they are not found in invertebrates (Noonan et al., 2004). The murine gene locus encoding α-Pcdhs comprises 14 variable exons, each of which is spliced to three α-cluster specific constant exons. The γ-Pcdh cluster encodes 22 different variable exons, similarly spliced to three γ-cluster specific constant exons (Tasic et al., 2002; Wang et al., 2002a). Each of the different variable exons harbors its own promoter and encodes the extracellular domain, transmembrane domain and a short portion of the intracellular domain (Tasic et al., 2002). The three constant exons of either α-, or γ-Pcdhs encode the constant intracellular domain of the protein. In contrast, the β-Pcdhs are encoded by 22 variable exons, lacking constant exons (Figure 1). The most striking feature of Pcdh organization is the similarity

with the immune system genes. Both the nervous system and the immune system are composed of enormously diversified cell types and undergo massive apoptosis, and the genes for the Pcdh family, as the genes for the Ig and T-cell receptor of the immune system are arranged in tandem arrays (Wu et al., 2001; Yagi, 2003). However, genomic rearrangement was not shown for the Pcdh gene cluster, as for the genes of the immune system. What was seen, though, for Pcdhs, is an increased mutagenesis rate during embryonic development which does suggest a possible role for somatic mutations in increasing variability of the Pcdh genes (Hirayama et al., 2001).

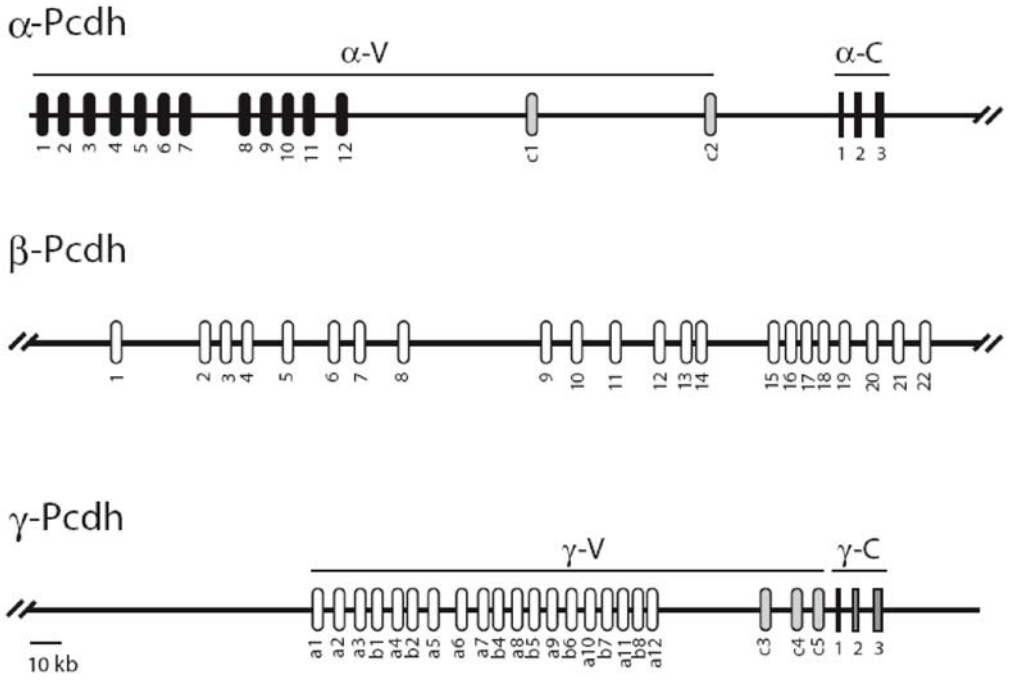

Figure 1. Clustered Pcdhs – genomic organization

The mouse gene cluster arrangement for the α-, β-, and γ-Pcdhs. Rounded squares display the different variable exons (α-V, β-V, γ-V) as arrayed on chromosome 18. Edged squares indicate the constant exons (α-C, γ-C) encoding the ICD (lacking in the β-Pcdh gene cluster). Scale bar is 10 kilobasepairs (kb).

The fact that functional α- and γ-Pcdhs result from the combination of distinct extracellular domains spliced to a common cytoplasmic domain suggests a mechanism in which distinct recognition events promote a common cellular response. Interestingly, structural differences between classic cadherins and Pcdhs support a role in signal transduction (vs. cell adhesion) for Pcdhs. Pcdhs lack the classic homodimerization motif,

resulting in weaker cell-adhesion capabilities. Thus, it has been suggested that Pcdhs may be more important in signal transduction than in cell adhesion (Morishita and Yagi, 2007, and references therein: Mutoh et al., 2004; Morishita et al., 2006).

1.3 Expression pattern of clustered Pcdhs in the brain

The unusual genomic organization of clustered Pcdhs raises the question of how these genes are differentially expressed in and during brain development. The mode of Pcdh expression is complex. In cerebellar Purkinje cells, single-cell RT-PCR analysis showed that individual cells express different numbers of α-Pcdh isoforms, all stemming from alternative splicing in a monoallelic fashion (Esumi et al., 2005). Interestingly, within the 22 γ-Pcdh variable genes, the γ-Pcdh A and B gene clusters share a similar mechanism of combinatorial monoallelic expression, but the C types are expressed in a bi-allelic fashion (Kaneko et al., 2006).

Frank et al. (2005), showed expression of γ-Pcdhs in the entire brain. The strongest expression was detected in cerebellum, hippocampus and olfactory bulb, but γ-Pcdhs were also detected in cortex, mid- and hindbrain, brainstem and spinal cord. Expression in general was highest in young post-natal animals (P1-3), and higher in young compared to adult animals (>P42).

Each of the different isoforms of γ-Pcdhs was detected in all brain regions. Interestingly, within regions, individual neurons displayed distinct γ-Pcdhs isoforms (Frank et al., 2005). A similar expression pattern was also shown for α-Pcdhs (Kohmura et al., 1998). These data strongly suggest a combinatorial monoallelic expression for Pcdhs in individual neurons.

On the sub-cellular level, Pcdhs are partially localized to synapses. In cultures, interneurons showed non-synaptic localization, in pyramidal neurons Pcdhs partially localized to synapses (Phillips et al., 2003). γ-Pcdhs are also found in biochemical fractions enriched in pre-synaptic proteins (“pre-synaptic web”; Phillips et al., 2001).

In conclusion, several properties of the Pcdhs make them good candidates for being involved in the task of wiring the brain. First, Pcdhs have a clustered genomic organization. This organization is similar to that of T-cell and B-cell receptors in the immune system, which provides a large variety of cell clones. Second, the combination of multiple extracellular domains with an invariant intracellular signaling domain, allowing to couple extracellular signals with a common intracellular signal. Third, expression predominantly in the CNS, and fourth, an association with synaptic membranes.

1.4 Post-translational processing of clustered Pcdhs

Pcdhs are type I transmembrane molecules and undergo sequential cleavage in the plasma membrane similar to other proteins such as Notch and APP (Schroeter et al., 1998; Ling et al., 2003). As a first step, the extracellular domain of the protein is released into the matrix by cleavage of the matrix metallo-protease ADAM10 (Reiss et al., 2006; Bonn et al., 2007). Consequently, in a second cleavage step, the γ-Secretase complex processes the protein within the plasma membrane, releasing the intracellular domain into the cytoplasm. The invariant, intracellular domain (ICD) is fastly degraded by the proteasome, as proteasome inhibitors cause accumulation of this fragment (Haas et al., 2005; Hambsch et al., 2005, Figure 2). The cleaved, soluble cytoplasmic domain of γ-Pcdhs has been shown to translocate to the nucleus where it may adopt signaling functions. Similar processing has recently been shown in our lab for α-Pcdhs (Bonn et al., 2007). The fate of the γ-ICD is of critical importance, as it is the intracellular signaling molecule shared by all γ-Pcdhs.

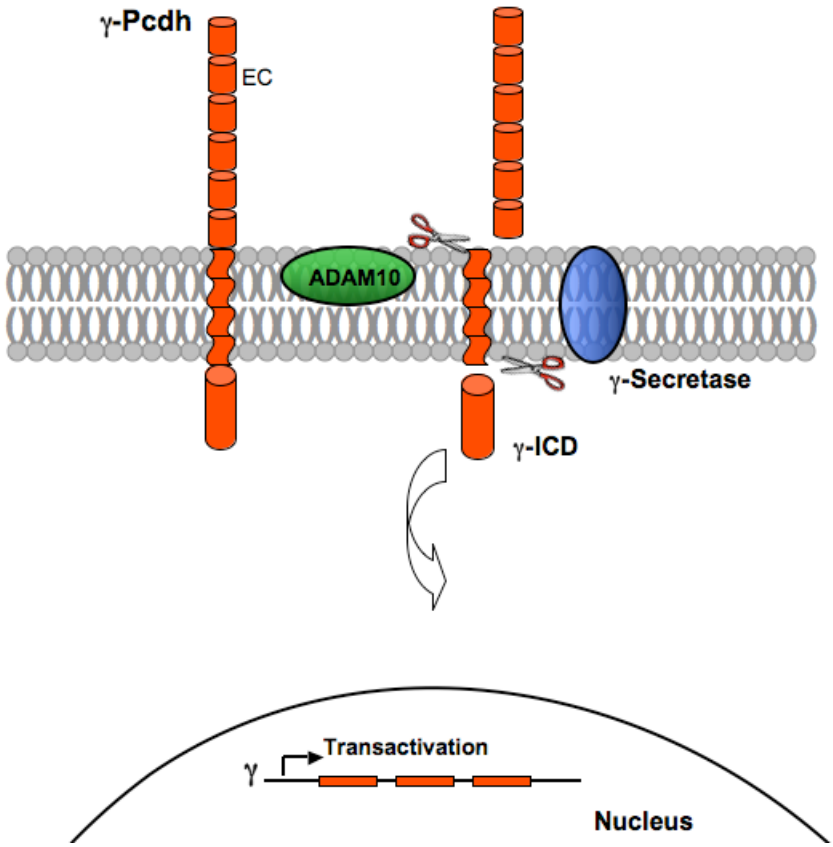

Figure 2. Intramembrane proteolysis of γ-Pcdhs

Schematic of γ-Pcdh protein in the plasma membrane prior to (left) and following (right) proteolytic cleavage by ADAM10 and γ-Secretase. The six EC domains are released into the extracellular matrix (red cylinders), whereas the γ-ICD (red clinder) translocates into the nucleus (arrow) where it transactivates endogenous γ-Pcdhs (black bent line, nuclear membrane; red rectangles, γ-Pcdh variable region exons; arrows in front of exons indicate individual γ-Pcdh promoter regions).

Signal transduction events, and possibly even transcriptional control, are likely mediated by the ICD and its interaction partners. One main fact that supports this hypothesis is the presence of a nuclear localization signal (NLS) in the ICD. Indeed, when α- or γ-ICD degradation is blocked by proteasome inhibitors, the ICD can be detected by immunostaining in the nucleus. Furthermore, luciferase assays showed transactivation of γ-Pcdh promoters upon overexpression of the γ-ICD (Hambsch et al., 2005; Bonn et al., 2007).

1.5 Transgenic mouse models for the research of γ-Pcdhs

The importance of γ-Pcdhs is underscored by the fact that deletion of the gene locus (Wang et al., 2002b), or deletion of the sequence encoding the ICD (Hambsch et al., 2005), both result in perinatal lethality. Spinal interneurons die at late stages of embryogenesis, causing lack of coordinated movement, and this is most likely the cause of perinatal death. Notably, spinal cord synapse numbers are also reduced. Other aspects of neurogenesis, neuronal migration, axon outgrowth and synapse formation still proceed in these mutants. When neurons from mutant spinal cord were cultured, they formed synapses, but then died, suggesting that γ-Pcdhs are necessary for the survival of specific neuronal subtypes. Data from global γ-Pcdhs knock-outs are difficult to interpret as the two main effects are the death of spinal interneurons, and a reduction in synapse number in the spinal cord, either of which could be caused by the other. It is very likely that death of neurons leads to a reduction in synapses connecting with other neurons. However, reduction of synapses may possibly occur first, leading to death of target neurons due to under-innervation (Wang et al., 2002b).

In an attempt to answer this question, mice were generated, deficient for both γ-Pcdh and Bax (Weiner et al., 2005). Bax is a pro-apoptotic protein, and the naturally occurring death of many neuronal populations is greatly diminished in the Bax knock-out mouse (Knudson et al., 1995). Surprisingly, although Bax deletion prevented death of spinal interneurons in γ-Pcdh knock-outs, it could not rescue perinatal lethality. Notably, numbers of both, excitatory and inhibitory synapses were still significantly reduced (30-50%). Similar phenotypes, including perinatal death, were seen in a hypomorphic allele where only part of the ICD was deleted (Weiner et al., 2005).

These findings support the hypothesis that synapse loss and consequently neuronal death may be a direct consequence of γ-Pcdhs deletion. Alternatively, Bax deletion might not prevent all aspects of neuronal dysfunction, as evident by the persistence of perinatal death. This highlights the need for a genetic model system in which the effect of γ-Pcdh mutations on synapse formation and maintenance can be tested in the context of an otherwise healthy organism.

In humans, only few mutations in non-clustered Pcdhs have been described (e.g., a mutation in Pcdh 15 which causes Usher syndrome; Alagramam et al. (2001). For clustered Pcdhs, only single nucleotide polymorphisms (SNPs) without detectable phenotypic consequence, and a deletion of several variable region exons of the α-Pcdh cluster, also without an overt phenotype, have been described (Miki et al., 2005; Noonan et al., 2003). The low number of described mutations, and the lack of any functional-loss mutations over such a large number of genes, points to a critical and indispensable role for these genes in human brain development.

1.6 Recent developments in γ-Pcdhs research; the use of conditional knock-outs

Recent studies have begun to address several of the main questions regarding γ-Pcdhs. Utilizing a conditional γ-Pcdh knock-out mouse in the retina, Lefebvre et al. (2008) were able to observe the effects of γ-Pcdhs deletion in a living mouse for several weeks, which was not possible in previous models (Wang et al., 2002b; Weiner et al., 2005). This led to the finding that at least in the retina, γ-Pcdhs were responsible for neuronal survival. When a conditional retina specific γ-Pcdh knock-out mouse was crossed with a Bax knock-out mouse to prevent apoptosis, neurons in the retina survived and synaptogenesis was almost completely normal. Response to focal light stimulation was unaffected. Additional findings demonstrated that the time window in which γ-Pcdh activity was necessary is very short, as elimination of γ-Pcdhs two weeks after birth showed no detectable phenotypic effects. This may indicate a role for the γ-Pcdhs in the development, but not the maintenance, of the retina (Lefebvre et al., 2008).

Lately, Prasad et al. (2008), have also utilized a conditional mutant, in which γ-Pcdhs were deleted in distinct parts of the spinal cord. Besides showing that spinal cord interneurons undergo exacerbated apoptosis, they have elegantly shown that apoptosis was non-cell autonomous. Migrating populations of interneurons displayed increased or normal levels of apoptosis, depending on the region to which they migrated. They found that mutant neurons did not demonstrate increased cell death, provided that they had

migrated into a region that expressed functional γ-Pcdhs, and wild-type cells displayed increased cell death in regions where γ-Pcdhs were deleted.

Taken together, Pcdhs exert a diverse range of functions, from protection against apoptosis in spinal cord and retina, to regulation of synapse development. Their roles in the cortex, however, are not yet understood.

1.7 γ-Pcdh interaction partners

Until recently, the signal transduction pathways, which mediate Pcdh activity, were entirely unknown. In a recent study trying to identify interacting intracellular downstream molecules of α- and γ-Pcdhs (Chen et al., 2008), the yeast two-hybrid system was utilized to screen for potential interaction partners. Two interesting proteins; PYK2 and FAK, both tyrosine kinases, were found. Interaction of α- and γ-Pcdhs with PYK2 and FAK inhibited their kinase activity, and overexpression of PYK2 could induce apoptosis in chicken spinal cord neurons. PYK2 activity was upregulated in γ-Pcdh deficient neurons. This was the first time that a signal transduction pathway has been associated with Pcdhs. The authors suggest that binding of PYK2 by Pcdhs would inhibit PYK2 apoptotic activity. Interestingly, both α- and γ-Pcdhs could inhibit PYK2, although they have different conserved domains. This suggests redundancy between the clustered Pcdhs, at least in some aspects of their function.

1.8 Virus-mediated transduction of neurons in neonatal brain

Almost all of the data described to this date for γ-Pcdhs were obtained for spinal cord neurons (with the exception of the retina; Lefebvre et al., 2008). Current models for γ-Pcdh research still lack some key features for the research of the functions of these proteins in higher brain functions, and new models need to be established. Mouse transgenic technology is currently the most reliable and well established method to study the functional importance of various genes *in vivo*. The generation of conventional transgenics, however, is a laborious and time consuming procedure. Preimplantation

embryos need to be harvested and manipulated *in vitro*. Transgenic animals are then generated by pronuclear injection of DNA into single-cell embryos. Usually tens of different transgenic founders have to be produced and subsequently bred with wild-type mice to establish a stable transgenic mouse line, expressing the transgene at sufficient levels and in the correct place. In many cases stochastic integration of exogenous DNA into the genome results in incorrect, early embryonic onset of expression, which is especially undesired if the exogenous gene product is likely to interfere with developmental processes (Capecchi, 1989a, b).

As an alternative to classic transgenic techniques, virus-mediated transgenesis, has been rapidly gaining favor. Recombinant adeno–associated virus (rAAV) type 8 vectors are exceptionally efficient for gene transfer to the CNS, where they transduce neurons and mediate long-term expression of transgenes. The efficiency of rAAV8 is presumably due to a ubiquitous receptor conferring wide ranging tropism and rapid release of vector genomes into the transduced cell nucleus (Broekman et al., 2006; Burger et al., 2005; Dr. Matthias Klugmann, personal communication). The specificity of virus-mediated neuronal transgene expression can be further improved by the use of neuron specific promoters, restricting expression specifically to different neuronal subtypes (Kugler et al., 2003). These unique characteristics identify rAAV8, in combination with appropriate promoters as a superior tool for either transducing a large neuronal population in the forebrain, or for systemically transducing defined brain areas, or even neuronal subpopulations, depending on the specific coordinates of viral injection.

In an attempt to achieve strictly postnatal expression in the brain of mice, we developed a rapid, reproducible and highly versatile method for expressing transgenes. Expression is achieved by rAAV8 mediated transgene delivery into the neonatal mouse brain at the first postnatal day (P0). This can be done either globally, or in a region specific manner.

1.9 Thesis objectives

The involvement of γ-Pcdhs in intracellular signaling and apoptosis during early development in the spinal cord encouraged us to study γ-Pcdh signal transduction pathways also in the adult mouse forebrain. We decided that the most direct way to

address this issue would be the identification of γ-Pcdh interaction partners in the mature brain *in vivo.*

As a first step, we immunoprecipitated γ-Pcdhs from mouse brain lysates, and used mass spectrometry to identify interaction partners. The interaction of various identified proteins was further validated by co-immunoprecipitation. Next, we managed to efficiently overexpress the γ-ICD, using targeted viral gene transfer in neonates. Electrophysiological recordings were finally used to uncover a novel phenotype of γ-ICD overexpression in inhibitory synapses in the cortex.

The overexpression of the γ-ICD in the brain, as well as the putative binding proteins *in vivo*, would allow us to obtain more information about the nature of their interaction. The novel phenotypes and proteins we have uncovered give us our first glimpse into the role of γ-Pcdhs in the cortex, and allow us a way to measure the effects of genetic manipulations *in vivo*. Our results represent ongoing research aimed at the elucidation of the role and function of the γ-Pcdhs in the brain, and the signal transduction pathways through which they exert their biological function.

2. Materials and methods

2.1 Antibody purification

A CNBr Sepharose purification column (Synaptic Systems, SySy) with 1000 µl of resin was first washed twice with PBS by gravity flow. Serum raised against the C-terminal domain of γ-Protocadherin was then loaded on the column (3-5 ml). The column was then washed three times with PBS, followed by an elution of the antibody with 0.1 M Glycine pH 2.2. In order to restore pH, different eluted fractions were collected in 1.5 ml eppendorf tubes containing 80 µl (10% elution fraction volume) or 120 µl of 1.5 M Tris pH 8.0. Elution fraction volumes were 800 µl for the first, and 1200 µl for another four elution fractions. Protein concentration was measured by a UV spectrophotometer at a wavelength of 280 nm. Western blotting and Coomassie staining were used to confirm that the majority of eluted antibody was present in the second fraction, at a concentration of about 0.3 mg/ml.

2.2 Antibody cross-linking to protein-A agarose beads

30 µl of Protein A Agarose Fast Flow Beads (50% v/v; Sigma-Aldrich) were washed twice in cross-linking buffer (25 mM HEPES pH 8.2, 150 mM NaCl) by inverting the tubes several times and subsequently centrifuged for one minute at 2500 RPM. Tubes were left on ice for one minute, then buffer was removed, leaving a small volume of buffer to prevent bead drying. 800 µl of fresh buffer was added to the beads together with 5 µg of the appropriate antibody (purified rabbit-anti-γ-Protocadherin, non specific rabbit IgG (Vector Laboratories), empty beads as controls). Tubes were rotated for two hours at 4°C to allow the antibody to bind to the beads. Excess antibody was removed and beads washed twice with 800 µl of fresh buffer. In order to covalently cross-link the antibody to the beads, Dimethyl pimelimidate·2 HCl (DMP, Pierce Biotechnology) was dissolved in cross-linking buffer at a final concentration of 10 mM (freshly prepared immediately before use). 500 µl of the DMP solution was added to the beads and rotated for 30 minutes at room temperature. Cross-linking reaction was terminated by addition of 200 µl

stopping buffer (0.5 M Tris pH 8.0), followed by 30 minutes rotation at room temperature. The cross-linking step was preformed twice. Beads were finally washed with 800 µl of 25 mM HEPES pH 7.4, 150 mM NaCl, 0.1% v/v Triton X-100. Buffer was removed and protein lysates added to the beads (see immunoprecipitation protocol). For calibration experiments, cross-linking efficiency was assayed by dot-blot procedure. Rabbit IgG was cross-linked to the beads, followed by low pH elution with 150 µl of 0.1% TFA. Serial dilutions (1-1:27) of the eluate were made and 16 µg bovine serum albumin (BSA, Fermentas) was added to 4 µl of each dilution to stabilize IgGs. Finally, 5 µl were pipetted onto a PVDF membrane. Secondary antibody was added and ECL reaction carried out as described for Western blotting (section 2.4).

2.3 Immunoprecipitation

Mice were deeply anesthetized using Isofluorane (Baxter), killed by decapitation, and brains removed quickly into pre-chilled lysis buffer containing 25 mM HEPES pH 7.4 and Complete™ protease inhibitor mix (Roche diagnostics GmbH). Protease inhibitors were not present in experiments destined for mass spetrometry analysis.

Brains were then homogenized using a glass homogenizer (S874 Potter). Lysates were incubated on ice for 10 minutes. All following steps were performed at 4°C. Lysates were centrifuged for five minutes at 2000 RPM in a Biofuge table-top centrifuge to remove cellular debris. Supernatant was diluted 1:2 with buffer containing 25 mM HEPES pH 7.4, 150 mM NaCl, and 1% v/v Triton X-100. The lysate was then rotated for one hour and centrifuged for 20 minutes (13000 RPM; 20000 RCF). Supernatant was precleared with 25 µl of non cross-linked Protein A agarose beads pre-washed twice with the same buffer, by rotating for 15 minutes. To remove beads, lysates were centrifuged for another 10 minutes (13000 RPM; 20000 RCF). Supernatant was collected and is henceforth referred to as the Input fraction of the immunoprecipitation. A sample was taken to quantify protein content with Bradford reagent (Bio-Rad Laboratories Inc.) vs. a standard curve of BSA (Fermentas) and read with a spectrophotometer at 595 nm (Pharmacia Biotech). 1.2 ml of lysate (4-5 mg/ml) were taken for immunoprecipitation, and mixed with 30 µl of Protein-A agarose beads cross-linked to the respective antibody.

Antibody-beads and protein mix were rotated overnight to allow binding. Antibodies used for immunoprecipitation were: purified rabbit anti-γ-Pcdh, rabbit IgG (Vector Laboratories Inc.), mouse anti-Sam68 (Santa Cruz Biotechnology, Inc.), goat anti-SLM-2 (Santa Cruz Biotechnology, Inc.), mouse anti-Flag (Sigma Aldrich).

The next day, beads were separated from the lysate by centrifugation at 2100 RPM for one minute. Supernatant was collected for analysis. Beads were washed by adding 900 µl of 25 mM HEPES pH 7.4, 150 mM NaCl, 0.1% v/v Triton X-100 followed by a one minute centrifugation at 2100 RPM, for 4 times. Buffer was carefully removed each time with a fine gel-loading tip, leaving a small volume of buffer to prevent bead drying. Specifically bound proteins were eluted from the beads by addition of 120 µl of 0.2% trifluoroacetic acid (TFA) in double distilled water (DDW), gentle shaking at room temperature for 30 minutes, and centrifugation for one minute (5000 RPM). Immunoprecipitations destined for mass spectrometry analysis were eluted twice in 150 µl, yielding 300 µl of total eluate fraction. Residual protein bound to the beads was collected by boiling with 300 µl 3 X SDS-PAGE sample buffer. Fractions were analyzed for the presence of γ-Pcdh protein by Western-blotting.

2.4 Western blotting

Protein lysates were separated by SDS-PAGE on 10% gels using standard conditions (Sambrook and Gething, 1989) and transferred onto PVDF membranes (0.45 µm, Amersham). Reactive bands were labeled by the following primary antibodies (Abs): Rabbit polyclonal antiserum against γ-Pcdh (1:1000) was generated by Eurogentech Laboratories from purified soluble γ-ICD-10-His protein as described (Hambsch et al., 2005), rabbit anti-GFP (1:5000, Abcam), rabbit anti-SLM-2 (1:4000, GenWay), mouse and rabbit anti-Sam68 (1:500, Santa Cruz Biotechnology, Inc.), mouse anti-c-Myc (1:500, Santa Cruz Biotechnology, Inc.), rabbit anti-Kir3.1 (1:1000, Alomone labs), rabbit anti-p38 (1:1000; Abcam), mouse anti-Flag (1:500, Sigma Aldrich). After incubation with peroxidase-coupled anti-rabbit/mouse secondary antibodies (1:5000; Amersham Biosciences), the blots were incubated with chemiluminescent reagents (Pierce), and photographic film was exposed to produce the results. Developed films of

immunoblots were scanned with a flatbed scanner, and digital images were imported and processed by Photoshop software (Adobe). Quantification of immunoblots was performed with ImageJ software (NIH).

2.5 Slicing and immunostaining

Mice were deeply anesthetized with Isofluorane (Baxter) and killed by decapitation. Brains were quickly removed and transferred to cold (4°C) 4% paraformaldehyde in PBS, pH 7.4 (PFA) and incubated overnight at 4°C. The following day, brains were washed several times with PBS, and then embedded in warm Agarose in PBS (3% w/v). Agarose blocks were then trimmed and glued onto a stage and placed in a vibratome (Leica VT1000S) and immersed in PBS. 100 μm sections were sliced and brain sections separated from the agarose with a sharp needle. Sections were incubated in blocking solution (5% normal goat serum (NGS), 1% Triton X-100, in PBS) for one hour. Primary antibody was added at the appropriate concentration (rabbit anti-GFP, 1:5000, mouse anti-NeuN, 1:1000, Millipore; in 1% NGS, 0.5% Triton X-100, in PBS) overnight followed by three washes of 10 minutes with PBS. Secondary antibody was added for two hours (anti-rabbit/mouse Cy-3 conjugated, 1:300 (Jackson Laboratories), or Alexa-fluor 488 conjugated, 1:400 (Invitrogen); in 1% NGS, 0.5% Triton X-100, in PBS). Sections were washed for three times in PBS (10 min) and transferred to 10 mM Tris pH 7.4 for ~5 minutes, and mounted on Superfrost plus slides (Thermo scientific) with Aqua Polymount (Polysciences).

2.6 X-gal staining

Vibratome sections were incubated in X-gal staining buffer (100 μl of 0.5 M K4Fe(CN)6, 100 μl of 0.5 M K3Fe(CN)6, 100 μl of 0.2 M MgCl2, 1 ml X-Gal (20 mg/ml), and 8.7 ml of PBS) for 1-24 hours at 37°C. Sections were washed 3 times in PBS for 10 minutes, and incubated for ~5 minutes in 10 mM Tris pH 7.4, and mounted on slides with Aqua Polymount (Polysciences).

2.7 Nissl staining

Vibratome sections were mounted on glass-slides and incubated for 30-60 seconds in Nissl solution (Thionin/Lauth's Violet, acetate salt, dissolved in 0.1M Acetic acid, 0.1M sodium acetate, final working concentration 0.1% w/v; Sigma-Aldrich). Slides were washed three times in DDW and dehydrated by incubation for several minutes in increasing ethanol concentrations (70%, 95% and 100% in DDW) and finally in Xylol. Slides were mounted with Eukitt-quick-hardening mounting medium (Fluka).

2.8 Virus purification

Recombinant Adeno associated viruses (rAAV) were purified by discontinous Iodixanol density gradient centrifugation. As described in Grimm et al. (1998), except that the helper plasmids used, expressed the rAAV8 envelope proteins (p179 and p220, Matthias Klugmann, Mainz University), resulting in rAAV8 pseudotype. Briefly, ten 15 cm HEK 293 plates were transfected with the appropriate plasmids (5 μg of the AAV construct, 5 μg of the p220 helper construct and 10 μg of the p179 helper construct). 48-72 hours after transfection cells were washed in PBS, and scraped in four ml of PBS and collected into a 50 ml Falcon tube. Cell suspensions were centrifuged for 10 minutes in a standard tissue culture centrifuge (Heraus Instruments; 800 RPM, 124 G) and the pellet was resuspended in 9 ml of 50 mM Tris pH 8.0, 150 mM NaCl. 500 μl of NaDOC (10% w/v) and 2 μl of Benzonase (500 units, Sigma-Aldrich) were added and tubes were incubated for 30 minutes at 37°C. Next, 584 mg of NaCl were added and tubes were incubated at 56°C for additional 30 minutes and then frozen at -70°C. Frozen cell lysates were thawed at 37°C and centrifuged for 30 minutes at 7000 RPM (6000 G) in a JA20 rotor in a Beckmann centrifuge. The virus containing supernatant was loaded on a discontinous Iodixanol gradient in ultracentrifuge tubes (70 Ti) as follows: 3 ml of 54%, 3 ml of 40%, 4 ml of 25% and 7 ml of 15% w/v. Approximately 9 ml of the cell lysate were added and centrifuged for 1.5 hours at 18°C in an ultracentrifuge (60000 RPM; 371,000 G). The

40% phase was collected with a syringe and diluted 1:2 in Magnesium and Potassium containing PBS (PBS-MK). The virus solution was then concentrated in an Amicon Concentrator (100 kDa) 3x at 2000xG to a final volume of 500 µl and filtered through a 0.2 mm Acrodisc filter. 10 and 20 µl samples were analyzed for viral protein amount and purity by SDS-PAGE.

2.9 Plasmids

γ-Pcdh A1-3X Flag was generated as a PCR fragment from a template (Bonn et al., 2007). The bidirectional promoter system and vector was described previously (Zhu et al., 2007). For cloning of the γ-Pcdh A1-3X Flag into this vector instead of the Venus protein, the γ-Pcdh A1 was amplified by PCR, the 3' primer containing a XhoI restriction site and the 3X Flag sequence (5' primer was: AACATGGCGATTCCAGAGAAGTTAACC; 3' primer was: CGGTCTCGAGTTACTTGTCATCGTCATCCTTGTAATCGATATCATGATCTTTAT AATCACCGTCATGGTCTTTGTAGTCCTTCTTCTCTTTCTTGCCCGA). The PCR fragment was restricted with XhoI on the 3' end. The bidirectional vector was prepared by restriction with BamHI and blunting with Klenow fragment, followed by restriction with XhoI, that released the Venus cassette and allowed the blunt-sticky (XhoI) insertion of the γ-Pcdh A1-3X Flag.

For insertion instead of Cre recombinase, a PCR fragment was amplified using the same template and 5' primer, and with a 3' primer that contained the 3X Flag sequence as before, but with a different restriction site (ClaI: Primer sequence was CGGTATCGATTTACTTGTCATCGTCATCCTTGTAATCGATATCATGATCTTTAT AATCACCGTCATGGTCTTTGTAGTCCTTCTTCTCTTTCTTGCCCGA). The vector was prepared in two steps, first by introduction of a ClaI restriction site containing oligonucleotide into the BclI site (oligonucleotide sequence was: GATCAATCGATTTAATTAAT), and then restriction in the EcoRV site on the 5' side, and ClaI on the 3' side, to release the Cre recombinase cassette and allow a blunt-sticky (ClaI) insertion of the γ-Pcdh A1-3X Flag.

In a third clone, γ-Pcdh A1 3X-Flag was cloned into a unidirectional rAAV vector encoding the human synapsin promoter fragment (Kugler et al., 2003) in two steps. First, oligonucleotides were designed which contained XhoI and AvrI restriction site sequences followed by the 3X Flag sequence (oligonucleotide sequence: CTCGAGCTTAAGCCTAGGGACTACAAAGACCATGACGGTGATTATAAAGATC ATGATATCGATTACAAGGATGACGATGACAAGTAA). The vector was restricted with BamHI and XhoI to release a pre-existing GFP-encoding cassette, and then blunted, and the oligonucleotides were ligated instead (blunt-blunt insertion). In the second step, γ-Pcdh A1 was amplified with primers containing overhangs encoding for the XhoI and AvrI restriction sites (5' primer: TTACTCGAGACCATGGCGATTCCAGAGAAGTTAACC; 3' primer: TTACCTAGGCTTCTTCTCTTTCTTGCCCGATTTC), and this PCR product was inserted using these sites. All cloning enzymes were purchased from Fermentas.

2.10 Electrophysiological recordings of miniature synaptic currents

Electrophysiological recordings of excitatory miniature post-synaptic currents (mEPSCs) in acute slices from the brains of virus-injected mice (8-9 weeks) were performed as in Pilpel et al. (2008) at a holding potential of -70 mV, except that 300 μm thick coronal slices were used. The region from which pyramidal neurons were selected (by morphology) corresponds to M1 motor cortex. Intracellular solution also differed and contained (in mM): Cs-Gluconate, 130, HEPES, 10, Phosphocreatinine, 10, Na-Gluconate, 10, Mg-ATP, 4, Na-GFP, 0.3, EGTA, 0.2, and NaCl, 4. For the recording of miniature inhibitory post-synaptic currents (mIPSCs), the cells were depolarized to a holding potential of +10 mV (liquid junction potential was not corrected, hence this corresponds to the equilibrium potential for AMPA receptor channels), and outward going currents (Cl^- ion entry through GABA receptors) were recorded. mEPSCs and mIPSCs are therefore recorded in the same cells.

3.Results

3.1 Analysis of γ-Pcdh interaction partners

γ-Pcdhs are transmembrane cell adhesion molecules, however, their intracellular signaling pathways are not known. It is therefore of key importance to elucidate the interaction partners of γ-Pcdhs. To date only two proteins that interact with the γ-ICD, FAK and PYK2, have been identified by yeast two-hybrid screens (Chen et al., 2008). The identification of additional proteins would give a broader understanding of γ-Pcdh intracellular signaling pathways. To this end, we decided to identify intracellular γ-Pcdhs interaction partners by immunoprecipitation from mouse forebrain lysates, Western blot verification of immunoprecipitation efficiency, and subsequent mass-spectrometry analysis.

3.1.1 Optimization of Western blot conditions

Previously in our lab, a polyclonal antiserum was raised against the entire C-terminal, constant intracellular domain of γ-Pcdhs. This antiserum specifically detects full-length γ-Pcdh in brain lysates (Hambsch et al., 2005). However, a significant level of non-specific background signals was apparent in Western blot analyses. Since mass spectrometry is a highly sensitive method (Hale et al., 2000), a reliable analysis of immunoprecipitated binding partners for γ-Pcdhs required substantial reduction of background signals. We therefore used an antibody purification protocol adapted from a commercial protocol (SySy, Goetingen, Germany). Indeed, purification of the antiserum greatly reduced non-specific background, as can be seen in Figure 3. The purified antibody was deemed sufficiently pure for our purposes. We continued further with the optimization of this antibody for the immunoprecipitation.

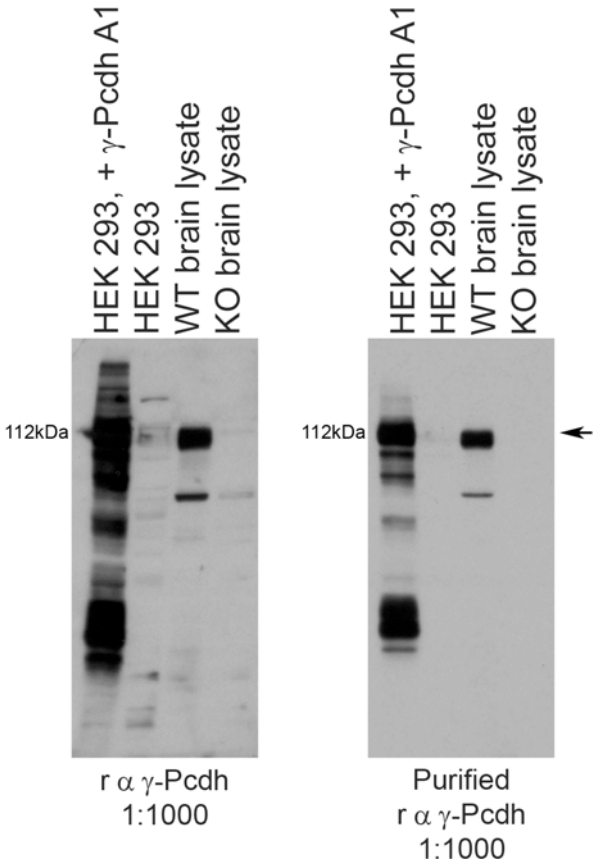

Figure 3. γ-Pcdh antibody purification

Left panel, Western blot probed with unpurified γ-Pcdh antiserum against HEK 293 cell lysates transfected (γ-Pcdh A1) or untransfected, and against P13 WT and P0 γ-Pcdh KO brain lysates, as indicated. Antibody dilution was 1:1000. Right panel, similar blot using affinity purified antisera. Note, the significant reduction of non-specific background bands in all 4 lanes. Arrow indicates molecular weight of full length γ-Pcdhs. 15 μg protein lysate was loaded in each lane. Molecular weight: kDa.

3.1.2 Optimization of immunoprecipitation conditions

Antigens may be differentially exposed in immunoprecipitation and Western blotting techniques. While Western blotting results in denatured proteins due to detergents and reducing chemicals in the loading buffer and gels, immunoprecipitation is performed under native conditions, in order to preserve non-covalent protein-protein interactions. While we have shown that the denatured epitope is recognized by the antibody, it was important to also verify that our purified anti γ-ICD antibody binds to the native protein and can be used to immunoprecipitate γ-Pcdhs from mouse brain lysates. In the next step we calibrated and optimized immunoprecipitation conditions in order to perform efficient and specific co-immunoprecipitation of γ-Pcdhs and their associated protein complexes.

We started by performing an immunoprecipitation experiment from wild-type (WT) brain lysates. Our objective was to obtain as much γ-Pcdh in the eluate fraction as possible. As can be seen in Figure 4, immunoprecipitation was indeed very efficient with our purified polyclonal antiserum. However, using boiling to detach γ-Pcdhs from the antibody-

beads-complex, we encountered another problem. A large amount of our antibody was also released into the eluate fraction, together with the γ-Pcdhs. An attempt to circumvent this problem by a different elution technique, the addition of a large excess of purified γ-ICD, was unsuccessful (data not shown). To prevent the release of antibody with the antigen, we decided to chemically cross-link with DMP the γ-ICD antibodies to the beads. Also, we changed the elution method from boiling to an elution in a low pH buffer to disrupt the antibody-antigen interaction. We tested different cross-linking protocols by dot-blot analysis (the most efficient of which is described in the Materials and Methods section; Figure 4 A). We thus established optimal conditions for the immunoprecipitation of the γ-Pcdh from brain lysates, using our polyclonal antibody.

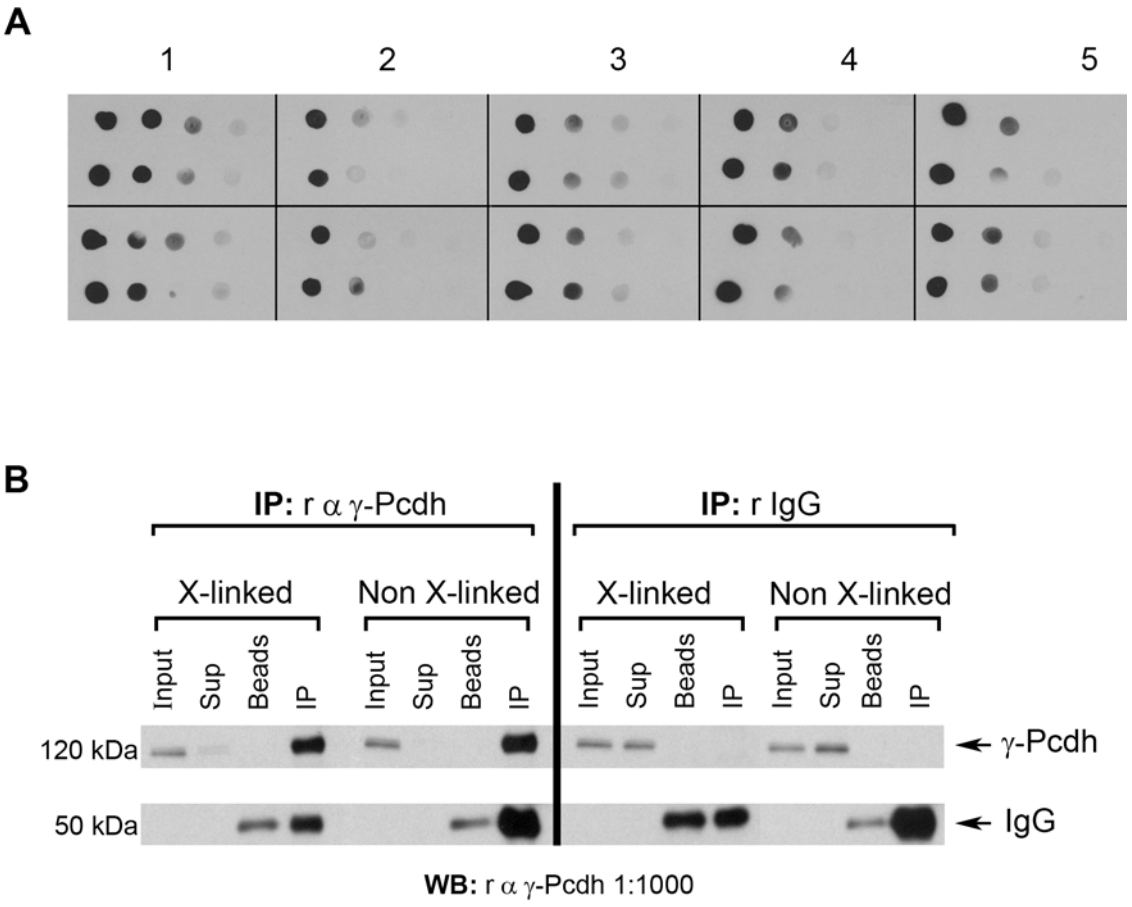

Figure 4. Optimization of immunoprecipitation protocol

A, dot blot analysis for different cross-linking (X-linking) conditions. 5 μg of rabbit antibody were eluted in 150 μl of TFA 0.1%, and 5 μl from this (representing ~3%) were blotted onto a PVDF membrane and followed up with a secondary antibody and ECL reaction. For better estimation of X-linking efficiency,

three more serial dilutions (1:3, 1:9, and 1:27) were performed, and all four conditions were blotted from left to right (Shown are two independent experiments in duplicates for each condition). The X-linking conditions were: 1, non X-linked; 2, Same X-linked for 30 minutes; 3. X-linked for 30 minutes with double amounts of DMP; 4, X-linking for one hour and 5, X-linked with double amounts of DMP for one hour. Efficient X-linking is indicated by weaker intensity of dots.. B. Immunoprecipitation (IP) performed under X-linking conditions vs. Non X-linking conditions. IP was performed either with the purified γ-Pcdh antisrum (left) or with rabbit IgG as control (right). Western blotting was performed with r α γ-Pcdh antibody. Input, supernatant (Sup), beads and IP fractions are shown. Top band (black arrow, 120 kDa) corresponds to γ-Pcdh band. Signal is detected in the input fraction and with higher intensity in the IP fraction (left). Right, signal is detected only in the input and sup fractions. Bottom bands show the heavy chain of the immunoprecipitating antibody (black arrow, 50 kDa), also detected by the secondary antibody. Signal is detected in beads and IP fractions. Under X-linking conditions, signal in the IP fraction is lower compared to Non X-linking conditions. Molecular sizes are given in kDa. WB, western blot.

3.1.3 Mass spectrometry analysis of co-immunoprecipitated proteins

After having established the optimal conditions for IP, we were ready for the next step in our analysis. We pulled down protein complexes from brains of newborn (P0), and adult (P42) mice (Figure 5). We chose the two ages with the expectation to find different associations of γ-Pcdhs with other proteins during CNS development (P0) and adulthood (P42). IPs were performed twice in duplicates for each age. All immunoprecipitated fractions were sent for mass-spectrometry analysis to our collaborator (Prof. Guus Smit at Vrije Universiteit in Amsterdam). As a negative control, we performed similar experiments with non-specific antibodies (rabbit IgG) and empty beads.

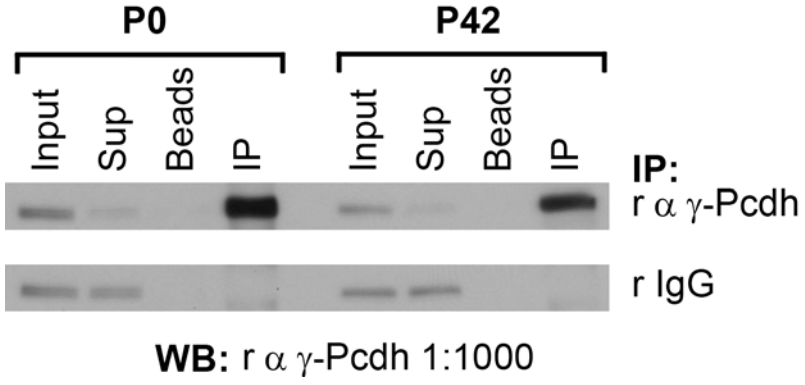

Figure 5. P0 vs. P42 immunoprecipitation of γ-Pcdhs

Top , comparison of IP efficiency from postnatal (P0), and young adult (P42) brains by western blot. Input, supernatant (Sup), beads and IP fractions are shown. 10 µl (0.08%) of brain lysate was loaded on a 10% protein gel (input and sup. fractions), and 10 µl of the IP fraction (0.8%, equivalent to 100 µl of the input fraction). Strongest signal is detected in the input and IP fractions, and only weak signal in the sup fraction in both ages. Bottom, IP with the control, non-specific rabbit IgG antibody. Signal is detected in the input and sup, but not in the IP fractions. Western blot was performed with the r α γ-Pcdh antibody. Molecular weight, kDa. WB, western blot.

For the analysis of specific interaction partners we then subtracted the non-specific interactors (rabbit IgG; beads alone) from our specific pull-downs (polyclonal anti γ-Pcdh antibody). The specifically interacting proteins from both age-groups are shown in Tables 1 and 2. As can be seen in the Tables both age groups yielded similar results. Almost all proteins detected in one age group were also detected in the other. This is perhaps not entirely unexpected. Mass spectrometry is a highly sensitive method capable of picking up minute amounts of protein. A developmental shift in the preference of binding partners would not necessarily be detected, as long as γ-Pcdhs are still capable of association with both "young" and "mature" proteins.

Table 1 **Proteins identified by IP and MS from P0 mouse brains**	**Total # of unique peptides**
>gi|18087749|ref|NP_291060.1|protocadherin gamma subfamily C, 4 [Mus musculus]	16
>SART3_MOUSE Squamous cell carcinoma antigen recognized by T-cells 3 - Mus musculus (Mouse)	12
>gi|148678187|gb|EDL10134.1|mCG133388, isoform CRA_q [Mus musculus]	12
>gi|148678172|gb|EDL10119.1|mCG133388, isoform CRA_b [Mus musculus]	12
>gi|18087755|ref|NP_291063.1|protocadherin gamma subfamily A, 2 [Mus musculus]	11
>KHDR1_MOUSE KH domain-containing, RNA-binding, signal transduction-associated protein 1 - Mus musculus (Mouse)	9
>gi|18087775|ref|NP_291073.1|protocadherin gamma subfamily A, 12 [Mus musculus]	6
>TM16H_MOUSE Transmembrane protein 16H - Mus musculus (Mouse)	5
>gi|18087743|ref|NP_291057.1|protocadherin gamma subfamily B, 7 [Mus musculus]	5
>gi|148678196|gb|EDL10143.1|mCG133388, isoform CRA_z [Mus musculus]	5
>gi|148678185|gb|EDL10132.1|mCG133388, isoform CRA_o [Mus musculus]	4
>gi|18087769|ref|NP_291070.1|protocadherin gamma subfamily A, 9 [Mus musculus]	4
>gi|18087757|ref|NP_291064.1|protocadherin gamma subfamily A, 3 [Mus musculus]	4

>ROA1_MOUSE Heterogeneous nuclear ribonucleoprotein A1 - Mus musculus (Mouse)	4
>gi|18087739|ref|NP_291055.1|protocadherin gamma subfamily B, 5 [Mus musculus]	4
>ROA2_MOUSE Heterogeneous nuclear ribonucleoproteins A2/B1 - Mus musculus (Mouse)	4
>FNBP4_MOUSE Formin-binding protein 4 - Mus musculus (Mouse)	4
>gi|18087753|ref|NP_291062.1|protocadherin gamma subfamily A, 1 [Mus musculus]	3
>gi|18087741|ref|NP_291056.1|protocadherin gamma subfamily B, 6 [Mus musculus]	3
>HNRPK_MOUSE Heterogeneous nuclear ribonucleoprotein K - Mus musculus (Mouse)	3
>gi|32451789|gb|AAH54741.1|Protocadherin gamma subfamily B, 1 [Mus musculus]	3
>gi|148747499|ref|NP_291065.3|protocadherin gamma subfamily A, 4 [Mus musculus]	3
>KHDR3_MOUSE KH domain-containing, RNA-binding, signal transduction-associated protein 3 - Mus musculus (Mouse)	2
>TBB4_MOUSE Tubulin beta-4 chain - Mus musculus (Mouse)	2
>gi|51092283|ref|NP_001003672.1|protocadherin alpha subfamily C, 2 [Mus musculus]	2
>LSM3_MOUSE U6 snRNA-associated Sm-like protein LSm3 - Mus musculus (Mouse)	2
>gi|26335715|dbj|BAC31558.1|unnamed protein product [Mus musculus]	2
>HNRPC_MOUSE Heterogeneous nuclear ribonucleoproteins C1/C2 - Mus musculus (Mouse)	2
>DPYL1_MOUSE Dihydropyrimidinase-related protein 1 - Mus musculus (Mouse)	2
>SRBS1_MOUSE Sorbin and SH3 domain-containing protein 1 - Mus musculus (Mouse)	2
>ADT2_MOUSE ADP/ATP translocase 2 - Mus musculus (Mouse)	2
>gi|50878294|ref|NP_291068.2|protocadherin gamma subfamily A, 7 [Mus musculus]	2
>BDH_MOUSE D-beta-hydroxybutyrate dehydrogenase, mitochondrial precursor - Mus musculus (Mouse)	2
>HNRPG_MOUSE Heterogeneous nuclear ribonucleoprotein G - Mus musculus (Mouse)	2
>ITAD_MOUSE Integrin alpha-D precursor - Mus musculus (Mouse)	2
>LSM4_MOUSE U6 snRNA-associated Sm-like protein LSm4 - Mus musculus (Mouse)	1
>LSM8_MOUSE U6 snRNA-associated Sm-like protein LSm8 - Mus musculus (Mouse)	1
>LSM2_MOUSE U6 snRNA-associated Sm-like protein LSm2 - Mus musculus (Mouse)	1
>RUXG_MOUSE Small nuclear ribonucleoprotein G - Mus musculus (Mouse)	1
>ADT1_MOUSE ADP/ATP translocase 1 - Mus musculus (Mouse)	1
>TBB2C_MOUSE Tubulin beta-2C chain - Mus musculus (Mouse)	1
>CALM_MOUSE Calmodulin - Mus musculus (Mouse)	1
>ATPA_MOUSE ATP synthase subunit alpha, mitochondrial precursor - Mus musculus (Mouse)	1
>gi|32451623|gb|AAH54555.1|Protocadherin gamma subfamily A, 8 [Mus musculus]	1
>IRK3_MOUSE G protein-activated inward rectifier potassium channel 1 - Mus	1

musculus (Mouse)	
>AT1B1_MOUSE Sodium/potassium-transporting ATPase subunit beta-1 - Mus musculus (Mouse)	1
>PANK4_MOUSE Pantothenate kinase 4 - Mus musculus (Mouse)	1
>gi|21426881|ref|NP_619603.1|protocadherin alpha 3 [Mus musculus]	1
>ELAV4_MOUSE ELAV-like protein 4 - Mus musculus (Mouse)	1
>NDUA4_MOUSE NADH dehydrogenase [ubiquinone] 1 alpha subcomplex subunit 4 - Mus musculus (Mouse)	1
>SMD1_MOUSE Small nuclear ribonucleoprotein Sm D1 - Mus musculus (Mouse)	1
>HNRPD_MOUSE Heterogeneous nuclear ribonucleoprotein D0 - Mus musculus (Mouse)	1
>CHKA_MOUSE Choline kinase alpha - Mus musculus (Mouse)	1
>DGKB_MOUSE Diacylglycerol kinase beta - Mus musculus (Mouse)	1
>K1967_MOUSE Protein KIAA1967 homolog - Mus musculus (Mouse)	1
>AP2A2_MOUSE AP-2 complex subunit alpha-2 - Mus musculus (Mouse)	1
>KIF27_MOUSE Kinesin-like protein KIF27 - Mus musculus (Mouse)	1
>LRC50_MOUSE Leucine-rich repeat-containing protein 50 - Mus musculus (Mouse)	1
>ELAV3_MOUSE ELAV-like protein 3 - Mus musculus (Mouse)	1
>gi|149262345|ref|XP_001478262.1|PREDICTED: hypothetical protein [Mus musculus]	1

Table 1

Mass spectrometry (MS) results for immunoprecipitated γ-Pcdhs binding proteins performed in P0 mice. Left column indicates the full ID of the proteins detected by MS, Right column indicates the total number of unique peptides detected for each protein, which is a measure of the level of confidence.

Table 2 **Proteins identified by IP and MS from P42 mouse brains**	**Total # of unique peptides**
>SART3_MOUSE Squamous cell carcinoma antigen recognized by T-cells 3 - Mus musculus (Mouse)	16
>gi|18087751|ref|NP_291061.1|protocadherin gamma subfamily C, 5 [Mus musculus]	11
>KHDR1_MOUSE KH domain-containing, RNA-binding, signal transduction-associated protein 1 - Mus musculus (Mouse)	10
>gi|148678187|gb|EDL10134.1|mCG133388, isoform CRA_q [Mus musculus]	8
>gi|18087775|ref|NP_291073.1|protocadherin gamma subfamily A, 12 [Mus musculus]	6
>STUB1_MOUSE STIP1 homology and U box-containing protein 1 - Mus musculus (Mouse)	6
>gi|148678196|gb|EDL10143.1|mCG133388, isoform CRA_z [Mus musculus]	5
>gi|18087755|ref|NP_291063.1|protocadherin gamma subfamily A, 2 [Mus musculus]	5
>gi|148678177|gb|EDL10124.1|mCG133388, isoform CRA_g [Mus musculus]	4
>IRK3_MOUSE G protein-activated inward rectifier potassium channel 1 - Mus musculus (Mouse)	4

>IRK9_MOUSE G protein-activated inward rectifier potassium channel 3 - Mus musculus (Mouse)	4
>BDH_MOUSE D-beta-hydroxybutyrate dehydrogenase, mitochondrial precursor - Mus musculus (Mouse)	4
>E41L3_MOUSE Band 4.1-like protein 3 - Mus musculus (Mouse)	3
>TBB5_MOUSE Tubulin beta-5 chain - Mus musculus (Mouse)	3
>gi|148678172|gb|EDL10119.1|mCG133388, isoform CRA_b [Mus musculus]	3
>gi|18087757|ref|NP_291064.1|protocadherin gamma subfamily A, 3 [Mus musculus]	3
>GHC1_MOUSE Mitochondrial glutamate carrier 1 - Mus musculus (Mouse)	2
>IRK6_MOUSE G protein-activated inward rectifier potassium channel 2 - Mus musculus (Mouse)	2
>TBB2B_MOUSE Tubulin beta-2B chain - Mus musculus (Mouse)	2
>gi|18700024|ref|NP_570954.1|isocitrate dehydrogenase 3, beta subunit [Mus musculus]	2
>TM16H_MOUSE Transmembrane protein 16H - Mus musculus (Mouse)	2
>gi|18087753|ref|NP_291062.1|protocadherin gamma subfamily A, 1 [Mus musculus]	2
>EAA2_MOUSE Excitatory amino acid transporter 2 - Mus musculus (Mouse)	2
>gi|50878294|ref|NP_291068.2|protocadherin gamma subfamily A, 7 [Mus musculus]	2
>GNAO1_MOUSE Guanine nucleotide-binding protein G(o) subunit alpha 1 - Mus musculus (Mouse)	2
>BANP_MOUSE Protein BANP - Mus musculus (Mouse)	2
>gi|44890274|gb|AAH66823.1|Pcdhgb7 protein [Mus musculus]	2
>AT1A3_MOUSE Sodium/potassium-transporting ATPase subunit alpha-3 - Mus musculus (Mouse)	2
>RSMN_MOUSE Small nuclear ribonucleoprotein-associated protein N - Mus musculus (Mouse)	2
>gi|86476054|ref|NP_001034474.1|VGF nerve growth factor inducible [Mus musculus]	1
>LYSCP_MOUSE Lysozyme C type P precursor - Mus musculus (Mouse)	1
>ROA3_MOUSE Heterogeneous nuclear ribonucleoprotein A3 - Mus musculus (Mouse)	1
>TBB2C_MOUSE Tubulin beta-2C chain - Mus musculus (Mouse)	1
>1433Z_MOUSE 14-3-3 protein zeta/delta - Mus musculus (Mouse)	1
>gi|3253071|dbj|BAA29046.1|CNR2 [Mus musculus]	1
>68MP_MOUSE 6.8 kDa mitochondrial proteolipid - Mus musculus (Mouse)	1
>gi|18087735|ref|NP_291053.1|protocadherin gamma subfamily B, 2 [Mus musculus]	1
>LSM8_MOUSE U6 snRNA-associated Sm-like protein LSm8 - Mus musculus (Mouse)	1
>RUXE_MOUSE Small nuclear ribonucleoprotein E - Mus musculus (Mouse)	1
>EAA1_MOUSE Excitatory amino acid transporter 1 - Mus musculus (Mouse)	1
>DNM1L_MOUSE Dynamin-1-like protein - Mus musculus (Mouse)	1
>NPTN_MOUSE Neuroplastin precursor - Mus musculus (Mouse)	1
>LSM3_MOUSE U6 snRNA-associated Sm-like protein LSm3 - Mus musculus (Mouse)	1
>MPCP_MOUSE Phosphate carrier protein, mitochondrial precursor - Mus musculus (Mouse)	1
>gi|18087769|ref|NP_291070.1|protocadherin gamma subfamily A, 9 [Mus musculus]	1

>gi|51092283|ref|NP_001003672.1|protocadherin alpha subfamily C, 2 [Mus musculus]	1
>CSR2B_MOUSE Cysteine-rich protein 2-binding protein - Mus musculus (Mouse)	1

Table 2

Mass spectrometry (MS) results for immunoprecipitated γ-Pcdhs binding proteins performed in P42 mice. Left column indicates the full ID of the proteins detected by MS, Right column indicates the total number of unique peptides detected for each protein, which is a measure of the level of confidence.

In order to assign the wide spectrum of proteins detected in our analyses to specific signaling pathways, the data need to be sorted within a logical framework. Thus, we divided γ-Pcdh interacting proteins of both age groups, into known signaling networks, and constructed a plausible interaction diagram (NCBI protein database, GeneCards database http://www.genecards.org/, and references therein for each protein) (Figure 6). Proteins of unknown biological function (e.g. TM16H) and proteins which could not be integrated into known signaling networks (e.g. ELAV), as well as some proteins with redundant functions (e.g. different GIRK proteins), are omitted from analysis for clarity. We also omitted proteins with ubiquitous functions such as Tubulin or Calmodulin. Our final interaction diagram represents, therefore, what we consider to be the most "physiologically sound" core interaction data. We were thus left with a workable number of proteins, which we next proceeded to test further for interaction with γ-Pcdhs.

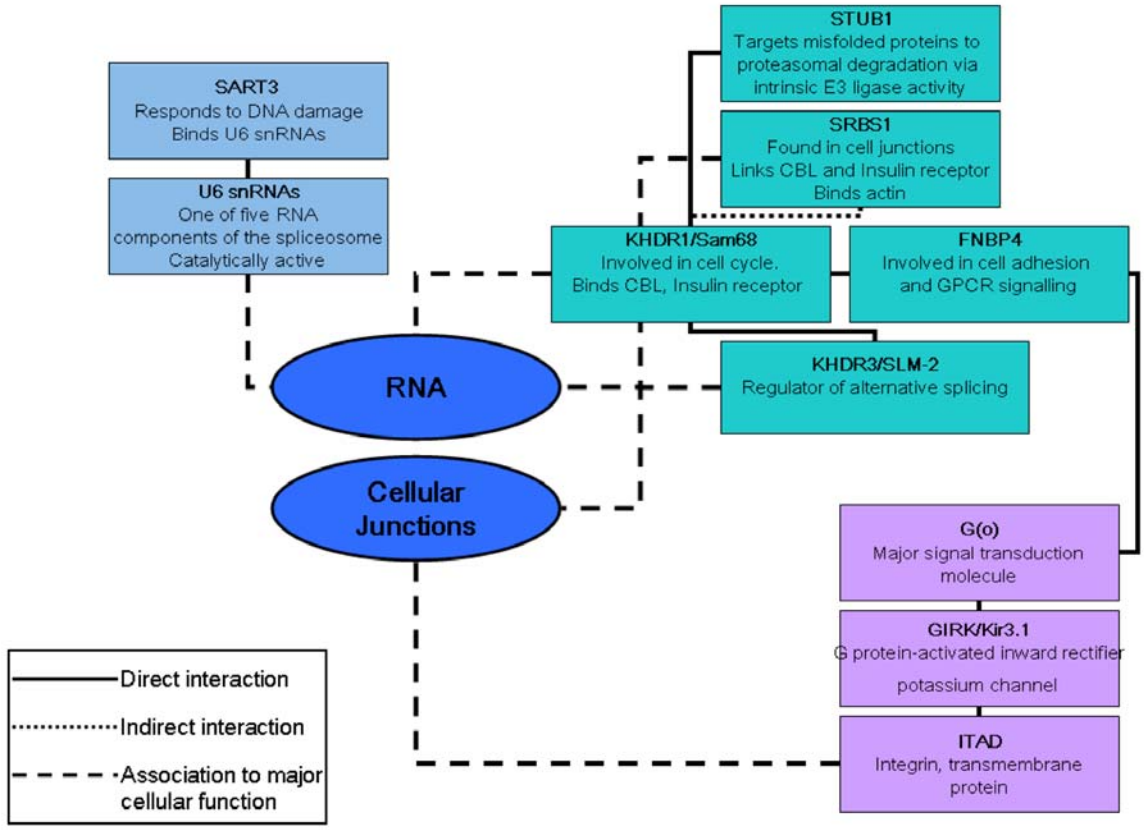

Figure 6. γ-Pcdh interacting proteins: functional grouping and known interactions

Diagram of γ-Pcdh interacting proteins sorted into functional groups according to their known biological function. Main groups shown contain the KH domain containing RNA binding proteins (Sam68 and SLM-2, and other associated proteins, light green rectangles), the G-protein coupled receptor channel Kir3.1 and G(o)-proteins (purple rectangles), and the splicing associated proteins such as SART3 (light blue rectangles). Elipses indicate major components of the cell (RNA and Cellular junctions) with which the different protein groups show an association (hatched lines between proteins known to associate with these functions and the function itself). Solid lines indicate a known direct protein-protein interaction. Dotted lines indicate an indirect protein-protein interactions.

3.1.4 Verification of mass spectrometry results using co-immunoprecipitation

The verification of any protein-protein interaction was essential for us to seriously consider a possible role for the binding proteins downstream to γ-Pcdhs. This is especially true for mass-spectrometry, as it is an extremely sensitive method leading to a high number of false-positive interactions. We therefore decided to corroborate mass-spectrometry data by use of biochemical tools. We first screened the publically available

antibody databases for commercial antibodies that can be used for co-immunoprecipitation. We chose antibodies for at least one protein in each of the 3 main interaction groups (Figure 6), which were: goat α SART3, goat α SORBS1, mouse and rabbit α Sam68, goat and rabbit α SLM-2, and rabbit α GIRK1/Kir3.1.

We first wanted to test whether we can efficiently use these antibodies to immunoprecipitate their respective antigens. We immunoprecipitated from mouse brain lysates as described before, and then performed Western blot analysis for the proteins. The manufacturer's instructions specified that the antibodies against SART3, SRBS1 and GIRK1/Kir3.1 do not work for immunoprecipitation, We could therefore only initially test immunoprecipitation for Sam68 and SLM-2. This was successful in both cases as shown, on the Western blot in Figure 7, albeit at a lower efficiency compared with immunoprecipitation preformed with the rabbit anti-γ-Pcdh antibody (as judged by a relatively large amount of non-immunoprecipitated protein in the Sup. fraction, and a weaker relative intensity of the IP band; Figure 7).

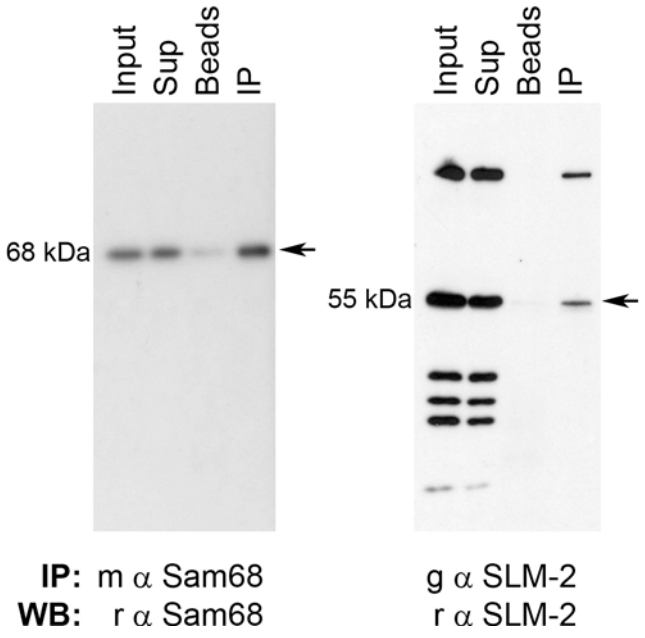

Figure 7. Immunoprecipitation of Sam68 and SLM-2

Western blot after IP from mouse brain lysates performed with m α Sam68 (left), and g α SLM-2 (right) antibodies. Immunoreactive bands were detected with r α Sam68 and r α SLM-2 antibodies, respectively. Input, supernatant (Sup), beads and IP fractions are shown. Left panel, signal is detected in all fraction, with highest intensity in the IP fraction. Right panel, signal is detected in the input, sup and IP fractions. Antibody specific bands are marked with an arrow. Molecular weight: kDa. WB: Western Blot. IP: Immunoprecipitation.

The critical question was whether we could co-immunoprecipitate the γ-Pcdhs together with the detected interaction partners. In the next step, we performed

immunoprecipitations with antibodies against Sam68 and SLM-2 and detected with the γ-Pcdh antibody, or vice-versa. For verifying the interaction of γ-Pcdh with the GIRK/Kir3.1 protein, we used the polyclonal anti γ-Pcdh antibody for immunoprecipitation, and the anti GIRK/Kir3.1 antibody for Western blotting detection. These experiments confirmed an interaction of γ-Pcdhs with Sam68, SLM-2, and GIRK/Kir3.1, as shown in Figure 8. We had also tried to immunoprecipitate using the anti γ-Pcdh antibody, and detect the SART3 and SRBS1 with specific antibodies, but Western blotting with these antibodies did not yield specific bands from mouse brain lysates (not shown).

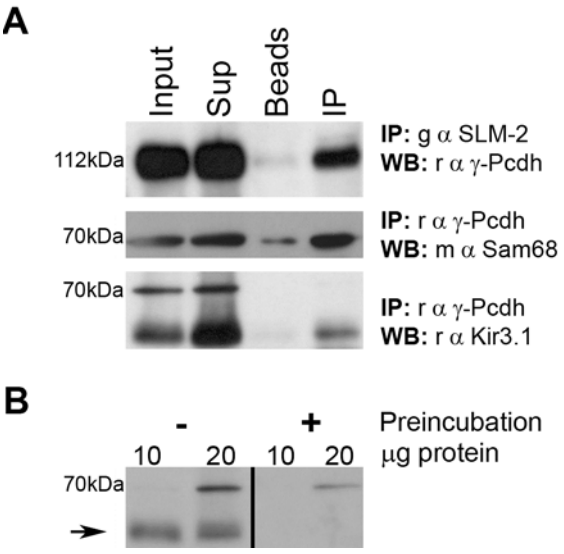

Figure 8. Co-immunoprecipitation of γ-Pcdh interacting proteins

Western blot analysis with one antibody following immunoprecipitation with other antibodies (Co-IP). A. Co-IP experiments for γ-Pcdhs with SLM-2 (top), Sam68 (middle), and Kir3.1 (bottom). Top panel, IP was preformed with the g α SLM-2 antibody and Western blot with the r α γ-Pcdh antibody. Middle panel, IP was preformed with the r α γ-Pcdh antibody and Western blot with the m α Sam68 antibody. Bottom panel, IP was preformed with the r α γ-Pcdh antibody and Western blot with the r α Kir3.1 antibody. Input, supernatant (Sup), beads and IP fractions are shown; immunoreactive bands can be detected in all fractions. B. Western blotting with the r α Kir3.1 antibody shows two bands (left, lane loaded with 20 μg lysate). Pre-incubation of the r α Kir3.1 antibody with the target (a Kir3.1-GST-fusion protein) eliminates the specific (lower) band (marked with an arrow). Molecular weight: kDa. WB: Western Blot. IP: Immunoprecipitation.

Taken together, our data verify the interaction of γ-Pcdhs with at least two functional protein groups, the KH domain containing, RNA binding proteins (Sam68 and SLM-2), and the G-protein coupled, inward rectifying potassium channels (GIRK/Kir3.1). At this point, we decided to attempt and ascertain the role of these protein interactions *in vivo*. To this end we needed to establish a way to deliver functional and putative binding

mutants of these proteins into the developing mouse brain, in order to establish the effect of these specific proteins and their interaction with γ-Pcdh on the development of brain circuitry and synaptogenesis.

3.2 Establishment of a method for transduction of neurons by targeted recombinant virus injections into neonatal mouse brains

As our main goal in this work was to study the intracellular signaling pathways of γ-Pcdhs *in vivo*, we required a highly reproducible, high throughput method to overexpress γ-Pcdhs and their interaction partners. To this end we have developed a rAAV based injection method, which allows us to transduce different regions in the brains of neonates (P0). This is especially important since γ-Pcdh knock-out mice die shortly after birth, precluding the analysis of signaling pathways in the postnatal brain. Viral induction in the neonate brain could be used to create a "viral" conditional knock-out of γ-Pcdhs, by injection of Cre recombinase expressing rAAV into the brains of a γ-Pcdh 2-lox line (*γ-Pcdh*^{2lox}). By applying this method we demonstrated that we could overexpress the full-length γ-Pcdh A1 protein, however more efficiently the constant intracellular domain of γ-Pcdh (γ-ICD) *in vivo* in the brain.

3.2.1 Establishment of targeted, reproducible injections into the neonatal mouse brain

The establishment of any reproducible system requires that one can compare different experiments. In order to standardize virus injections into the P0 mouse brain we first generated a neonatal brain atlas (for C57/Bl6) to establish coordinates for exact targeting of the injection needle into different brain regions (Figure 9). Such a brain atlas already exists for adult mice (Paxinos et al., 1980), but not yet for neonates.

We fixed whole heads from newborn mice in 4% PFA, stained coronal and saggital sections (200μm) with Nissl dye (see Materials and Methods) and serially arranged them on microscope slides (Figure 9 A). These sections constitute a miniature brain atlas that

can be used for injection into neonatal mice. Most major structures are visible from the Nissl staining (e.g. hippocampus, ventricles, olfactory bulb).

In order to determine the coordinates for needle insertion into the different brain regions we utilized the well defined Lambda demarcation, clearly visible on top of a neonatal mouse, as morphological landmark (Figure 9) and calculated the anterior/posterior (A/P), medial/lateral (M/L) and dorsal/ventral (D/V) distances to target different brain structures (Figure 9).

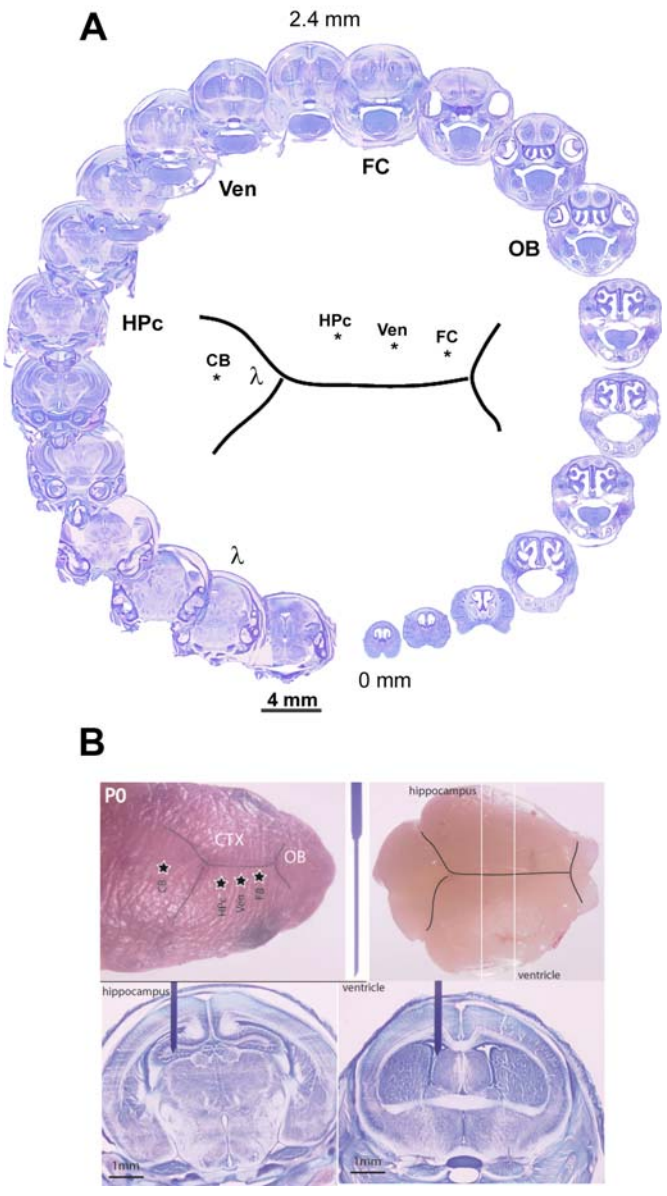

Figure 9. Mouse P0 brain atlas

A. Nissl stained, 200µm thick, serially arranged coronal sections of a P0 mouse head are arranged in a circle. Schematic diagram in the center of the circle illustrates the lambda demarcation (λ) and the coordinates for targeted frontal cortex (FC), ventricular (Ven), hippocampal (HPc) and cerebellar (CB) injections, marked with asterisks. Distances and scale bar are given in mm; HPc, hippocampus; Ven, ventricle; FC, frontal cortex; CB, cerebellum; OB, olfactory bulb; λ, lambda.

B. Top panels, dorsal view of a P0 mouse head and brain with the main brain sutures drawn to scale on top. Asterisks indicate the rostro-caudal points of needle insertion. Right side, shows the actual proportions of a 33 gauge bevelled needle used for targeted virus injections. Bottom panels illustrate the respective coronal brain sections for hippocampal and ventricular injection, with the needle superimposed in the precise injection location drawn to scale for visualization. P0, postnatal day zero; CB, cerebellum; CTX, cortex; OB, olfactory bulb.

As the volume of virus-containing solution and the speed of injection are critical parameters for efficient infection, we constructed an injection setup by utilizing a standard WPI infusion-pump, controlling a 50 µl syringe connected with plastic tubing to a "needle holder" equipped with a 34 gauge beveled needle (Figure 10). The injection speed was controlled by a standard WPI controller operated with a foot switch. To determine the correct D/V position (depth) of the needle-tip, we marked the endpoint on the needle with a water-resistant pen. We have thus obtained the necessary equipment, coordinates, and demarcations, to drive viruses into specific regions of the neonatal mouse brain.

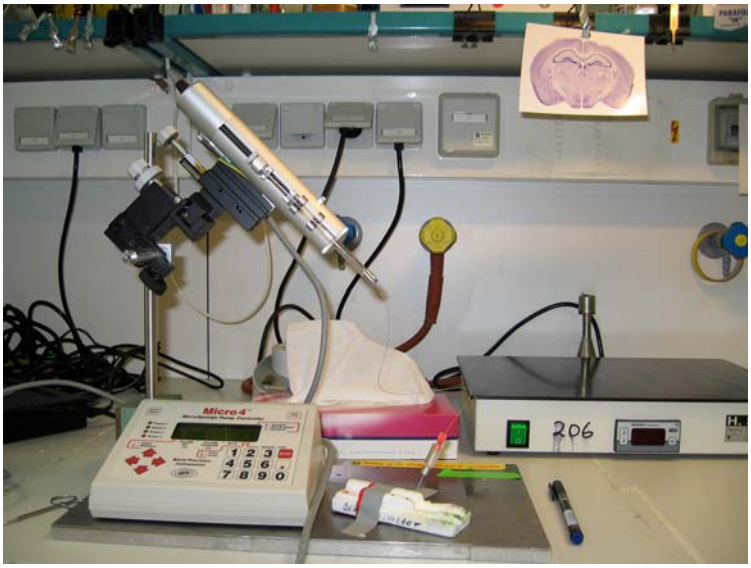

Figure 10. Injection setup
Picture of the P0 virus injection setup. Left side, microinjection pump holding a 50 ml syringe, and digital control panel from WPI. Right side, heat plate used for restoring body temperature and normal circulation to the pups. Styrofoam pup holder used to immobilize anesthetized pups during injection, and injection needle connected by thin tubing to the pump are shown right to digital control panel. Also shown is a felt-tip pen used for marking the injection site on the head surface. Foot pedal is not shown.

3.2.2 Characterization of virus-infected brain regions

When using viruses to deliver transgenes into the brain, the question arises is as to how well different regions can be targeted. In order to test the targeting specificity and virus diffusion upon ventricular, hippocampal, olfactory bulb and cerebellar injections, we used heterozygous *Rosa26*$^{+/-}$ neonates injected with rAAV8 pseudotyped virus expressing Cre-recombinase under the control of a human synapsin core promoter/enhancer element. Cells carrying the 'stop-floxed' Rosa26 reporter allele turn dark blue after Cre-mediated recombination and subsequent X-gal staining (Soriano, 1999). Before injections, newborn heterozygous *Rosa26*$^{+/-}$ pups (2-5 hours after delivery) were separated from the mother

and wrapped for 3-5 minutes in a paper towel covered with wet-ice to anesthetize and immobilize them. Immediately thereafter, pups were placed onto a custom made 'styropore mold' to fix them into an appropriate position for subsequent virus injections. 1 or 2 μl of purified rAAV8 (10^{11} genomes/ml) containing solution were infused into the lateral ventricles (from Lambda:1 mm rostral, 1 mm lateral, 1.5 mm ventral; n=10), 0.5 μl of rAAV8 into the hippocampus (from Lambda: 2 mm rostral, 0.7 mm lateral, 1.8 mm ventral; n=8) or 1 μl of rAAV8 into the cerebellum (from Lambda: 1 mm caudal, 2 mm ventral; n=6) of neonates at a speed of 125 nl/sec, through a 34 gauge beveled needle. After injections, the needle was kept in place for additional ~3 seconds to avoid backflow of virus containing solution. The speed of the injection and the width of the needle were both important, as faster injection speed and/or thicker needles resulted in significant backflow of virus-solution through the injection channel, immediately after removal of the needle. Following injection, the pups were placed on a 37°C warming plate for recovery. After all newborns were fully motile, they were returned to their mother as a group. In most cases the mother accepted the injected pups and fostered them. Injection of a typical litter (6-10 pups) took about 15-20 minutes. Three weeks after injection, mice were genotyped and *Rosa26*$^{+/-}$ mice were used to determine infection and targeting efficiency after vibratome sectioning and subsequent X-gal staining.

Figure 11 shows X-gal staining in Rosa26 pups on brain sections (100 μm) after targeted virus delivery into different brain regions. Ventricular injection with a high-titer virus resulted in efficient infection of the entire dorsal forebrain, hippocampus, and some cells in the olfactory bulb (Figure 11 A). Additionally, we tested different virus titers, which enabled us to control the density of infection (Figure 11 B,C). Our results show that targeted injection can be used to achieve efficient infection of selected brain regions such as hippocampus (Figure 11 D), olfactory bulb (Figure 11 F), and cerebellum, yet the latter was not efficiently transduced upon ventricular injections (Figure 11 G).

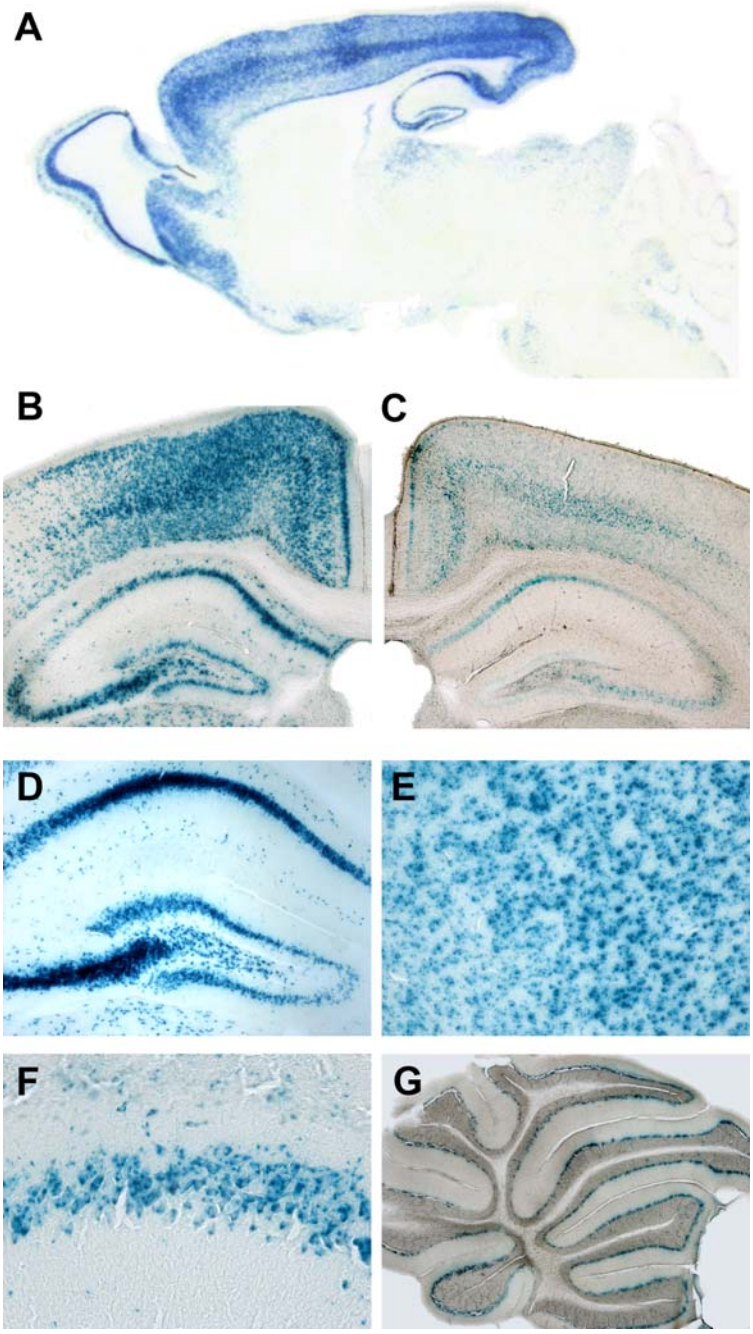

Figure 11. Efficient infection of selected brain areas

A. X-gal stained (blue) parasaggital section of a heterozygous Rosa26$^{+/-}$ mouse brain after ventricular P0 rAAV8.Syn.Cre (2µl, 1x10^{8} particles/µl) injection. Robust staining can be detected in all dorsal forebrain structures and the mitral cell layer of the olfactory bulb. B. Coronal section (-2mm from bregma) showing robustly infected cortex and dorsal hippocampus after ventricular injection at P0 with 2µl (1x10^{8} particles/µl) and in C sparse infection of a corresponding region infected with 2µl (1x10^{7} particles/µl) of rAAV8.Syn.Cre. D. Staining of a coronal brain section after targeting the dorsal hippocampus at P0. E. High magnification image of a heavily infected cortical region shown in B demonstrating the maximum density of infection. F. Staining of a saggital section through the mitral cell layer of the olfactory bulb at high magnification. G. Staining of a saggital section through the cerebellum demonstrating the selective transduction of Purkinje cells after cerebellar targeting at P0. In all cases mice were sacrificed 21 days after virus delivery.

In summary, we were now able to inject either specific brain regions, or the entire neocortex. This affords us a powerful tool for specific and global “viral transgenics”.

3.2.3 Onset and duration of fluorescent protein expression

As our interests lie in the function of γ-Pcdhs in the developing mouse brain, we had to determine how early expression from the viral constructs can be detected. To determine the exact onset and duration of protein expression after rAAV8 mediated gene transfer into P0 mouse brains, we injected virus expressing a Venus fluorescent reporter protein driven by the human synapsin core promoter/enhancer element into the lateral ventricles as described above. Brains from injected mice were removed and PFA-fixed, 24, 48 hours, seven days, and 4 months after virus injection (Figure 12). Coronal sections were stained with a polyclonal antibody against GFP to increase detection sensitivity for subsequent analysis under a fluorescent microscope. Fluorescent cortical neurons could be readily detected as early as 24 hours after virus delivery, though fluorescence intensity and numbers of infected cells increased with time (Figure 12). A related issue that we considered had to do with the fact that rAAV remains in an episomal state, and does not integrate into the host genome, raising the question whether virus DNA will remain stable in neurons after a long time period. To answer this question, we monitored fluorescent protein expression during puberty and adulthood. Figure 12 E illustrates robust long-lasting expression of the Venus reporter protein up to 4 months after injection. No obvious loss of Venus fluorescence was detected in the cortex when compared with comparable cortical regions stained at earlier time points. These experiments demonstrate fast, efficient and long-lasting expression of a fluorescent reporter-protein after rAAV8 mediated transduction of neonatal mouse brain neurons. The very early onset of expression allows us to use this system to study the developmental aspects linked with γ-Pcdhs.

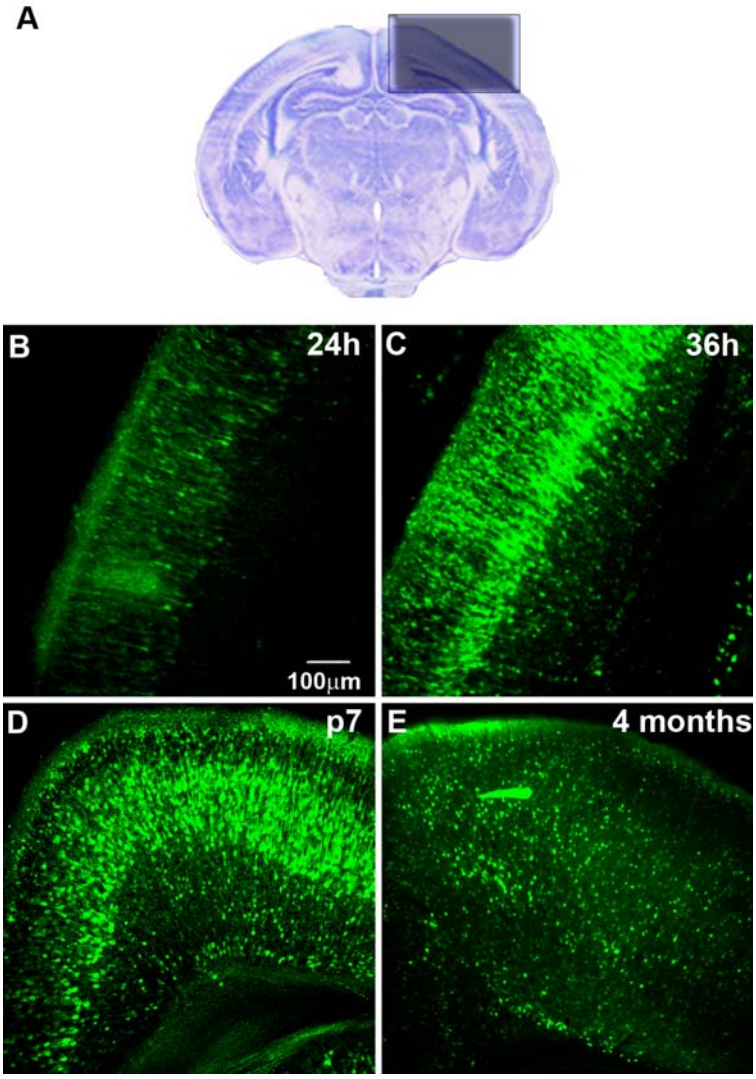

Figure 12. Timecourse of viral expression

A. Coronal brain section of P0 mouse at the approximate focus of injection. Overlayed window illustrates the general region from which the following images were taken. B. Anti-GFP stained coronal section of the dorsal cortex 24 hours after ventricular rAAV8.Syn.EGFP delivery at P0 showing the first appearance of fluorescently labeled neuronal cell bodies mainly in upper cortical layers. C. Same after 36 hrs. D. The intensity of fluorescence as well as the number of labeled neurons in the cortex increase with time, reaching a maximum of infection at ~P7. Note that at P7 fluorescently labeled neurons and their neurites are clearly visible also in deep cortical layers. E. Robust fluorescent labeling is still present 4 months after virus delivery. Scale bar is 100μm.

3.2.4 Virus distribution after parenchymal injection into the neonatal brain

Our data on proteins interacting with γ-Pcdhs were obtained using immunoprecipitation from WT mice. This requires a relatively large and homogenous region of expression in the brain. To this end, we needed to determine the volume of the tissue that could be dissected and analyzed after efficient viral transduction. To investigate virus diffusion around the injection site into the parenchyma of the frontal cortex (from Lambda: 3.5 mm anterior, 0.5 mm lateral, 0.7 mm ventral; n=5) we bilaterally delivered 1 μl rAAV8 (10^{11} genomes/ml), expressing the fluorescent Venus reporter protein with an injection rate of

80 nl/sec. Forty two days later, 100 μm thick coronal sections were analyzed for Venus expression. Figure 13 A shows the distribution and density of Venus expressing neurons ~2 mm from injection site along the A/P axis of the brain. Note that no fluorescent neurons could be detected in the hippocampus, thus excluding possible miss-targeting of virus into the lateral ventricles. The density graph depicted in Figure 13 G shows the infection density as a function of the distance from the injection point. These data demonstrate that a region of 1mm around the injection site can be efficiently transduced upon parenchymal injections. Most notably, the number and position of infected neurons are highly reproducible (n=5); differences in virus spread and infection efficacy between different mice injected into similar coordinates were not significant. In summary, focal, targeted expression can be achieved upon injection of rAAV8 into the brain parenchyma. The areas transduced span a significant portion of the mouse forebrain and should contain enough exogenous protein for biochemical analyses.

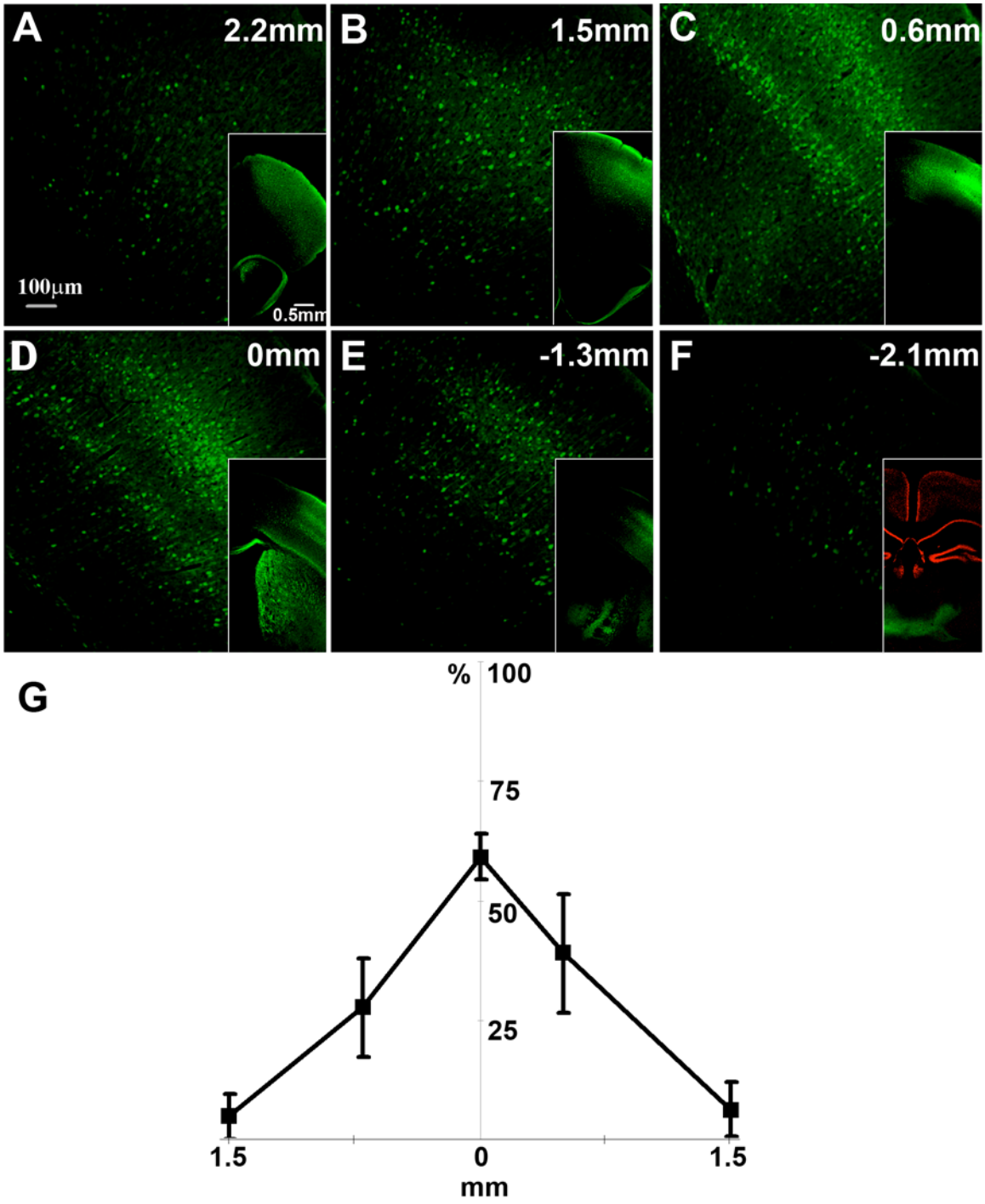

Figure 13. Virus distribution after forebrain injection

A-F. Anti GFP stained coronal sections of the frontal cortex 42 days after ventricular rAAV8.Syn.EGFP delivery at P0. Fluorescently labeled neurons can be detected 2.2mm from the injection spot (inset shows an overview of the area; A), with increasing density of fluorescent neurons at 1.5- (B, inset) and 0.6mm (C, inset). Highest viral transduction can be seen at the point of virus delivery (D, inset). The number of infected neurons decreases again linearly with -1.3- (E, inset) and -2.1mm (F, inset) distance from injection

spot. Inset in panel F shows that the dorsal hippocampus (stained against NeuN in red) was not infected by the virus. Scale bar is 500μm. G. Quantification of infection efficacy as a function of the distance from the injection point. At 0 mm (injection point) ~60% of all neurons express EGFP (number of virally transducted green fluorescent neurons divided by the total number of neurons identified by NeuN staining). The number of virally infected neurons decreases linearly on both sides with increasing distance from the point of injection.

3.2.5 Expression of full-length γ-Pcdh in the neonatal mouse brain

The viral delivery system described above enabled us to overexpress proteins in the neonatal mouse brain. In our immunoprecipitation experiments, we used a polyclonal antibody directed against the γ-ICD. This has the drawback that the binding of the antibody to the γ-Pcdhs might mask some of the intracellular interactions we were searching for. Alternatively, excess antibody may compete with the endogenous binding proteins for the binding sites on the surface of the γ-ICD. We therefore attempted to overexpress γ-Pcdh A1 in a tagged version and immunoprecipitate it with a specific antibody directed against the tag. A triple-Flag tag was fused to the C-terminus of γ-Pcdh A1 (γ-Pcdh A1-3X Flag). We used the rAAV-based bidirectional tetracycline regulated expression system described in Zhu et al. (2007). Using this approach, we wanted to replace the endogenous γ-Pcdh with the exogenous tagged version, by injecting the virus into the γ-Pcdh 2-lox mouse line in combination with a Cre recombinase expressing rAAV. The original bidirectional vector encodes a Venus fluorescent protein and the Cre recombinase, bidirectionally controlled by a tetracycline-transactivated minimal promoter (Figure 14 A1). Expression of both proteins is initiated by co-injection of an activator virus that expresses the tetracycline dependent transactivator (tTA) under the control of a neuron specific promoter (Zhu et al., 2007). We first replaced Venus with γ-Pcdh-A1-3X Flag, in order to create the replacement vector encoding both the tagged exogenous γ-Pcdh, and Cre recombinase (Figure 14 A2). However, no Flag tag signal could be detected after this construct had been injected into neonatal mouse brains, although Cre recombinase was (not shown). A possibility which we considered was that the bidirectional promoter displays a preference of expression to one side, thus favoring the expression of one cassette. To test this hypothesis, we also cloned the γ-Pcdh-A1-3X Flag

instead of the Cre recombinase (Figure 14 A3). In this construct we obtained Venus fluorescence but no Flag signal was detected here either. We attribute this to the relatively large size of γ-Pcdh-A1 (112kDa), which may bias relative expression levels using this system.

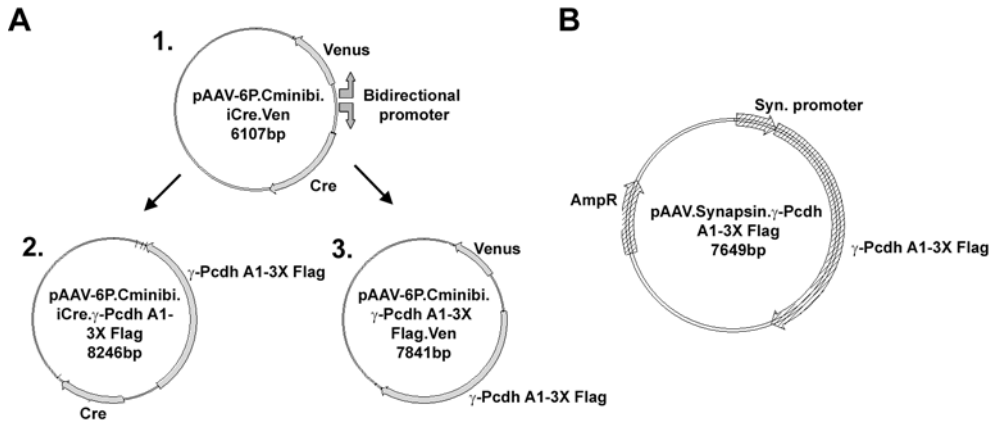

Figure 14. Vectors used for virus mediated expression of γ-Pcdh A1

A. Original plasmid from Zhu et al. (2007) (1). The bidirectional minimal promoter drives expression of the Venus fluorescent protein and Cre recombinase in opposite directions. (2) Venus cassette replaced by γ-Pcdh A1-3x Flag or (3) Cre recombinase cassette replaced by γ-Pcdh A1-3x Flag. B. Unidirectional vector from Kugler et al. (2003) γ-Pcdh A1-3X Flag expressed under the control of the human synapsin promoter. AmpR, Ampicillin resistance cassette. Molecular sizes in bp.

As an alternative approach, we utilized a unidirectional vector and cloned the sequence for γ-Pcdh-A1-3X Flag downstream of the human synapsin promoter. The synapsin promoter that we used was shown to drive expression specifically in principal neurons using the rAAV gene delivery system (Kugler et al. (2003), Figure 14 B). As this vector does not contain a fluorescent marker, we injected rAAV8.Syn.γ-Pcdh-3X Flag together with a rAAV8 expressing the red fluorescent Tomato reporter protein under the same promoter. We succeeded to detect γ-Pcdh-A1-3xFlag using a specific antibody directed against the triple Flag tag (monoclonal anti-Flag antibody). Furthermore, the fluorescent Tomato signal and Flag immunostaining overlapped completely, demonstrating efficient expression of two proteins in the same neurons, which may also be used to co-express Cre (Figure 15 A-C).

In order to establish an endogenous γ-Pcdh replacement system, we had to verify that we obtain enough exogenous protein, and are able to immunoprecipitate it from injected brain lysates. We injected brains with the virus encoding the tagged γ-Pcdh A1, and attempted to immunoprecipitate it with the commercial Flag antibody. As can be seen in Figure 15 D (lower panel), we managed to efficiently immunoprecipitate γ-Pcdh-A1-3X Flag. However, the amount of tagged immunoprecipitated γ-Pcdh-A1-3X Flag was very small, compared to endogenous γ-Pcdh (Figure 15 D; compare intensity of Input fraction in the left upper panel and the IP fraction). In summary our data indicate that low molecular weight proteins are much more efficiently expressed using this method. We therefore tried to use it for expressing the putative signaling domain of the γ-Pcdhs, the γ-ICD. We first used local injection and immunostaining for the γ-ICD in order to visualize overexpression *in vivo*. To this end, we also decided to raise specific monoclonal antibodies as our polyclonal antibody is not suitable for these purposes.

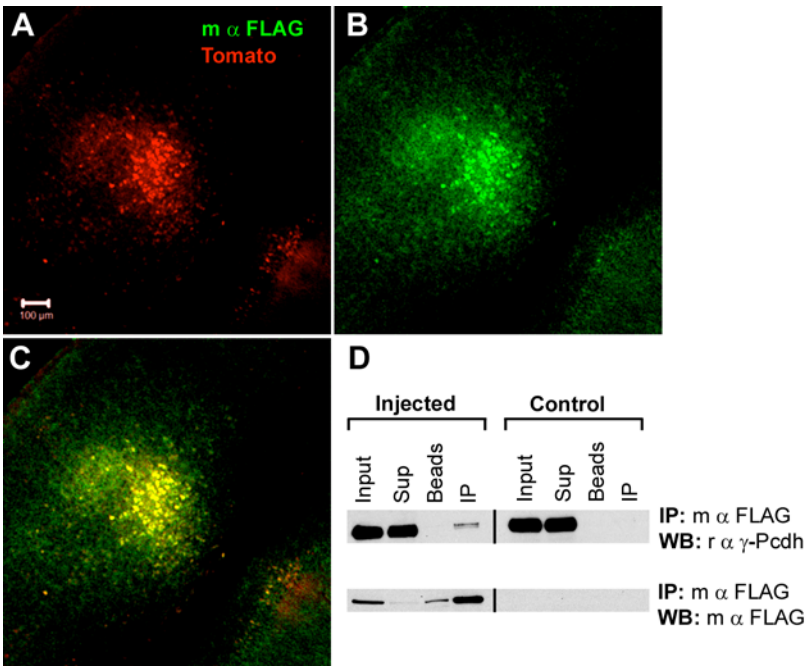

Figure 15. Targeted expression of γ-Pcdh A1-3X Flag in cortex by neonatal injection

A-C. Fluorescent Images of coronal sections from mice after injection with γ-Pcdh A1-3X-Flag and 'Tomato' expressing viruses. Red channel shows Tomato expression (A). Green channel shows immunostaining of γ-Pcdh A1-3X Flag tag (B). Co-localization (yellow) can be seen in the overlay of both channels (C). Scale bar is 100 µm. D. Western blot following imunnoprecipitation from mouse brain lysates three weeks after neonatal virus injection, compared to non injected control, using the monoclonal anti-Flag antibody; input, supernatant (Sup), beads and IP fractions are shown. Top panel: Western blotting using r α γ-Pcdh; endogenous levels of γ-Pcdhs are unchanged by viral expression of γ-Pcdh A1, as can be seen by comparing the input fractions between injected and control

mouse brain lysates. IP fraction from injected mouse using the monoclonal anti-Flag antibody shows a weak band. No signal is detected in the IP fraction of the control mouse. Bottom panel: Western blot with the monoclonal anti-Flag antibody shows signal in all fractions of the injected mouse. IP fraction shows highest signal intensity indicating efficient pull down. No signal is detected in fractions from the control mouse. WB: Western Blot. IP: Immunoprecipitation.

3.2.6 γ-ICD injection and staining in brain using specific monoclonal antibodies

Overexpression of the γ-ICD differs conceptually from replacement of the full-length protein. A high level of overexpression is required to yield a dominant phenotype. Our polyclonal antibody cannot be used for immunostaining (not shown). We therefore raised monoclonal antibodies targeted against the γ-ICD together with Synaptic Systems (SySy, Goettingen, Germany). Next, we injected a virus encoding the γ-ICD (rAAV8.Syn.c-Myc-γ-ICD.IRES.Venus) into WT mice in order to overexpress the protein. For seeing whether we could detect endogenous levels of γ-Pcdh, we used a virus encoding Cre (rAAV8.Syn.Cre.IRES.Venus) and injected that into *γ-Pcdh*^{2lox} mice in order to reduce endogenous γ-Pcdhs to a minimum. As a control, WT mice were also injected with the Cre encoding virus. Both viruses also encode a Venus marker. Brains were sliced and stained in parallel with the different monoclonal anti γ-ICD antibodies (12 clones). One of these clones (no. 317) showed positive results in immunostainings of brain sections (Figure 16). Using this antibody we could detect overexpressed γ-ICD, but not endogenous levels of γ-Pcdh (no difference was seen between WT and *γ-Pcdh*^{2lox} injected mice). Based on our results we suspect that the antibody may not be sensitive enough to detect endogenous protein over the background. Alternatively, endogenous levels of the γ-Pcdhs may be very low. γ-ICD was, however, very efficiently overexpressed.

For immunoprecipitation of the γ-ICD it would be preferable to have a monoclonal antibody, as the chances that it would mask putative interaction zones is lower than a polyclonal antibody, since it only has a single recognition epitope. In addition, the use of different antibodies for the immunoprecipitation and subsequent Western blotting prevents the unwanted detection of non-specific heavy chains of the immunoprecipitating antibody. We therefore also tried to immunoprecipitate γ-Pcdhs from WT brain lysate

using the monoclonal γ-Pcdh antibody. Figure 16 D shows that we achieved efficient immunoprecipitation.

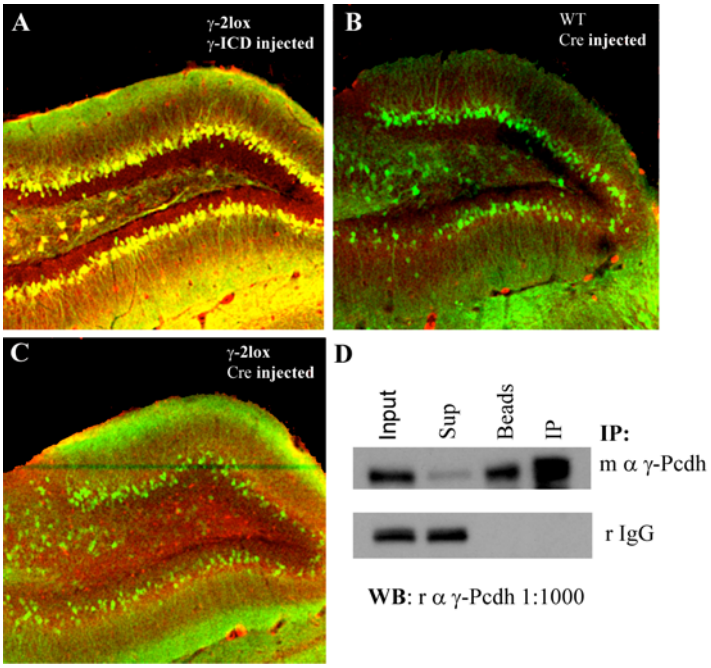

Figure 16. Immunostaining and immunoprecipitation using monoclonal anti γ-Pcdh antibodies

A-C. Coronal sections of the Dentate Gyrus (DG) showing an overlay fluorescent image of Venus (green) and immunostaining signal with monoclonal antibody (clone number 317) raised against the γ-ICD (red). A. Coronal section of the DG from a γ-Pcdh^{2lox} mouse injected with a virus expressing the γ-ICD shows intense co-labeling (yellow) in neurons. B. WT mouse injected with a virus encoding the Cre recombinase was used as a control to visualize endogenous γ-Pcdh imunostaining levels. Immunostaining signal is very weak (red). C. Deletion of endogenous γ-Pcdhs by injection of a Cre recombinase expressing virus into γ-Pcdh^{2lox} neonate. Immunostaining intensity is not visually distinguishable from WT control slices (B). D. Western blotting following immunoprecipitation using monoclonal anti γ-Pcdh antibody from WT brain lysate; input, supernatant (Sup), beads and IP fractions are shown. Top panel, IP with the m α γ-Pcdh antibody. Signal is detected in all fractions, IP fraction shows highest intensity. Bottom panel, IP with the control antibody (non-specific rabbit IgG). Immunoreactive signal is detected for the input and sup fractions only. Western blotting was preformed with the r α γ-Pcdh antibody. WB: Western blot, IP: Immunoprecipitation.

In conclusion, the production of monoclonal antibodies has afforded us a tool for improving immunoprecipitation of γ-Pcdhs and immunodetection of virally overexpressed γ-ICD in brain slices.

3.2.7 Successful overexpression of the C-terminal domain γ-Pcdh in P0 mice

Our expression data show that we can express large proteins such as the full-length γ-Pcdh, but only at a low level. In light of this, we decided to overexpress only the small putative signaling domain of the γ-Pcdhs, the γ-ICD. This was done with the rationale that a high level of overexpression may yield a phenotype from which we could extrapolate an endogenous function. Our data for smaller proteins like GFP and Cre recombinase were obtained from immunostained brain sections. We therefore needed to be able to estimate the extent of overexpression in comparison to the WT. We therefore injected rAAV8 expressing γ-ICD into the ventricles of P0 WT pups, followed by a "booster" injection at P2 to infect more cells. Twenty days later mice were sacrificed and protein lysates were prepared from their forebrains, and probed for the presence of the γ-ICD. As can be seen (Figure 17 A), in 3/3 cases, this resulted in significantly higher γ-ICD levels compared to uninjected controls. The viral plasmid that we used contained a c-Myc tagged version of the γ-ICD, followed by an internal ribosomal entry site (IRES) and a Venus encoding cassette (Stefan Bonn, doctoral thesis, 2007). Western blots against the c-Myc tag and against the Venus protein clearly show that most of the γ-ICD we detected in the injected brain lysates originated from our construct. In addition, levels of the full-length γ-Pcdh were similar in injected and control animals (Figure 17 A). We were also interested to see if we could pull down the overexpressed γ-ICD. We performed immunoprecipitation on injected brain lysates as described above. As shown in Figure 17 B, the overexpressed γ-ICD could be efficiently immunoprecipitated. Since we could demonstrate that we can effectively overexpress the γ-ICD in high levels and retrieve it under native conditions, we were ready to proceed to the next step, measuring physiological effects of γ-ICD overexpression in the cortex.

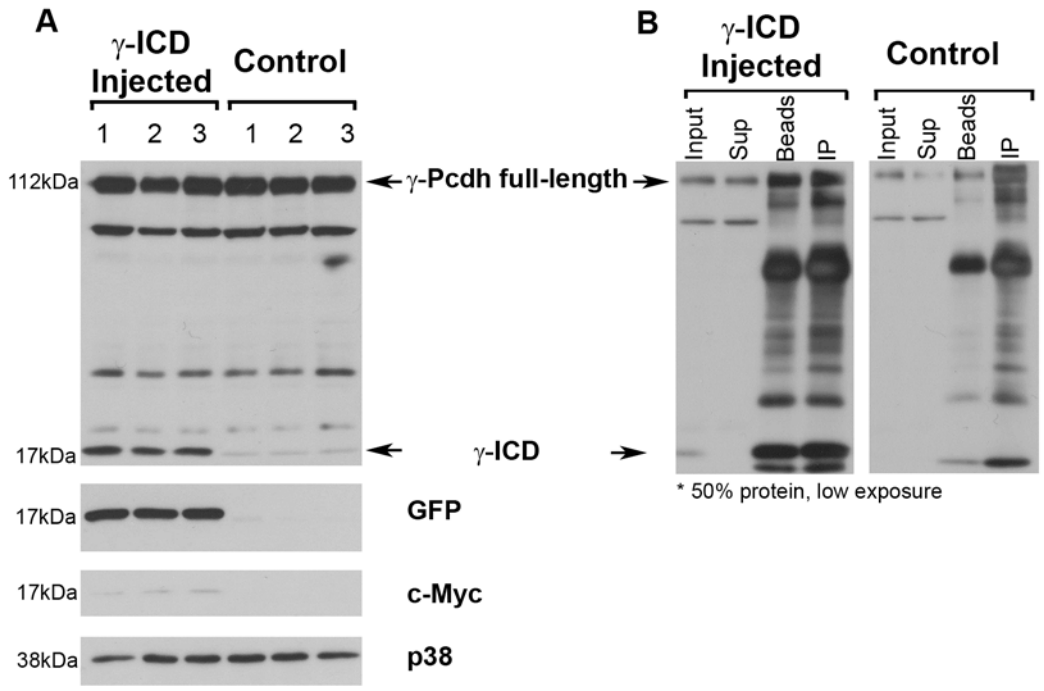

Figure 17. Efficient overexpression and immunoprecipitation of γ-ICD in mouse forebrain after ventricular injections

A. Comparison of the immunoreactive band after WB of brain lysates from newborn mice injected in the ventricles with rAAV8.Syn.c-Myc-γ-ICD IRES.Venus (P0 and booster P2) and from non-injected litter mate controls. Western blot analysis was performed against γ-Pcdhs (top panel), GFP (second from top), c-Myc (second from bottom), and p38 MAPK as loading control (bottom). While full-length γ-Pcdh levels were unchanged in injected mice (indicated by arrow, top), the small molecular weight γ-ICD was highly overexpressed (indicated by arrow, bottom). B. Western blot after immunoprecipitation of overexpressed γ-ICD; input, supernatant (Sup), beads and IP fractions are shown. Signal for the full length γ-Pcdh (top arrow) can be seen in all fractions of injected (left panel) and non injected control mice (right panel). Highest intensity is seen in the IP fraction. γ-ICD signal (bottom arrow) is higher in injected mice (left panel) than in the non injected control (right panel). Highest intensity is seen in the IP fraction of both mice. In order to avoid over-exposure of the signal from the concentrated IP fraction, 50% total protein amounts (compared to A) were loaded. (exposure less than 30 seconds).

3.2.8 Physiological effects of γ-ICD overexpression in principal cortical neurons

We were interested in observing the effects of γ-ICD overexpression on synaptic properties of virally transduced cells in the cortex, a region of the brain that is most

associated with higher cognitive functions, and displays intricate interconnectivity and plasticity.

We injected P0 WT mice with rAAV8 expressing γ-ICD. The human synapsin promoter in this vector restricts expression to principal neurons (Kugler et al., 2003). We set out to measure the effect of this overexpression on the post-synaptic compartment in these neurons. The most straightforward method to do this is to record miniature synaptic currents by inhibiting spontaneous firing with tetrodotoxin (TTX). We performed recordings under conditions which enabled us to record both miniature excitatory, and inhibitory, post-synaptic currents in voltage clamp configuration (mEPSCs and mIPSCs, respectively). Surprisingly, while mEPSC amplitudes were entirely unchanged in neurons from virus injected vs. control mice (Figure 18 A,B), mIPSC amplitudes of the same neurons were greatly increased (mean values were 11.6 ± 0.71 pA vs. 9.6 ± 0.29 pA, N=13 and 12 cells from injected vs. control mice, respectively. $P < 0.02$, T-test. Figure 18 C,D). Frequency of mIPSCs was higher in injected mice, though not significant (225 ± 86.9 vs. 61 ± 27.3 events per minute for injected vs. control mice. $P > 0.08$, T-test). Frequency, however, is very variable and increases in frequency are usually concurrently detected with increases in amplitude because of more miniature events that pass above detection threshold (7.5 pA).

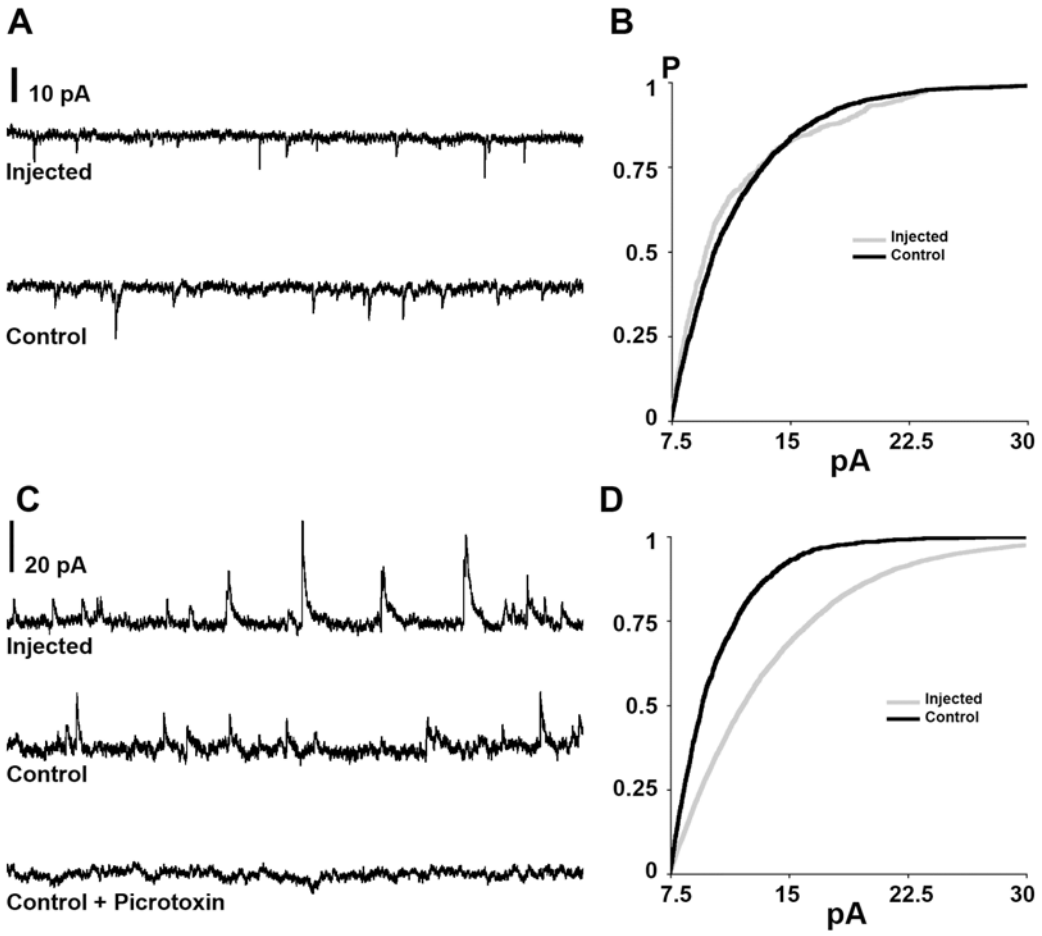

Figure 18. Increased miniature inhibitory post-synaptic currents in γ-ICD overexpressing cells

A. Sample traces recorded at a -70 mV holding potential of cells from injected (top trace) and control mice (bottom trace). Negative deflection in the current trace are individual mEPSCs. Scale bar is 10 pA. B. Cumulative histograms of mEPSC amplitude distributions for injected (grey) and control (black) groups overlay each other; no difference was detected between the groups. C. Sample traces recorded at a +10 mV holding potential from the same cells shown in A (top and middle trace correspond to cells from injected, and WT control mice, respectively). Positive deflections of the current trace are individual mIPSCs. Note that mIPSCs are significantly larger in amplitude in the injected group. The bottom trace is the current trace from the same control cell (middle trace), after perfusion of picrotoxin into the recording chamber and inhibition of GABA receptors in order to demonstrate that all recorded events are indeed GABA receptor-mediated currents. Scale bar is 20 pA. D. Cumulative histograms of mIPSC distribution shows a clear increase of mIPSC amplitudes in neurons from injected mice vs. controls.

This is the first physiological effect mediated by γ-Pcdhs in the adult cortex. The large difference in amplitude distribution of the mIPSCs which is a mostly post-synaptic property, together with the fact that our viral vector targets exclusively excitatory neurons, strongly support a role for the γ-ICD in shaping the inhibitory post-synapse.

Taken together, these data show that we can overexpress the small molecular weight γ-ICD protein, well above endogenous levels. We can also immunoprecipitate it and this may enable us to study also weaker interactions, for example, between the γ-ICD and proteins that bind to it in a transient manner. Furthermore, the overexpression of the γ-ICD induces a physiological synaptic phenotype, which corroborates the validity of this technique for the advancement of γ-Pcdhs research.

In conclusion, the expression of the γ-ICD using our viral delivery system in neonates will hopefully allow us to achieve this overexpression in large regions of the brain, and observe physiological, morphological and behavioral phenotypes that may give us together with our biochemical findings a window to the function of γ-Pcdhs in brain complexity.

4. Discussion

4.1 γ-Pcdh structure and processing suggests a role in signal transduction

γ-Pcdhs are essential for survival since mice lacking the gene locus encoding them (or the γ-ICD) die shortly after birth (Wang et al., 2002b; Hambsch et al., 2005). Lack of γ-Pcdhs has been associated with interneuronal death (Wang et al., 2002b; Weiner et al., 2005), but other than that the function of these proteins remains unknown. The γ-Pcdhs have variable extracellular domains, and their combinatorial expression in individual cells generates variation, resulting in unique Pcdh a "signature" in each cell. In contrast to the variability of their extracellular domains, there is only one α- and one γ- cluster specific intracellular domain, the ICD. It was this domain and its functional connotation, which interested us most. Various polymorphic extracellular domains, combined with one conserved intracellular domain, suggest a role in signal transduction that might be very simple, perhaps even binary. A good example for binary signaling, postulated in Chen et al. (2008), is neuronal survival vs. apoptosis, mediated via inhibitory binding of γ-Pcdhs to PYK2, and thus its seclusion. PYK2 is a kinase whose activity in interneurons of the spinal cord leads to cell death. When inhibition of this kinase by the γ-Pcdhs is relieved, PYK2 is released and the cell undergoes apoptosis.

Importantly, γ-Pcdhs undergo presenilin dependent intramembrane proteolysis (PS-IP) to release the constant γ-ICD. This is achieved by consecutive proteolysis of two proteases: ADAM10 and the γ-Secretase complex (Haas et al., 2005; Hambsch et al., 2005; Reiss et al., 2006). Notably, ADAM10 and the γ-Secretase complex are also responsible for cleavage of several other important proteins such as Notch, APP, as well as the classic N- and E-cadherins (Lammich et al., 1999; Hartmann et al., 2002; Maretzky et al., 2005; Reiss et al., 2006). For these proteins as well as for others (e.g ErbB-4 and SREBP-1), the intracellular fragment has been shown to mediate intracellular signaling (Weidemann et al., 1989; Brown and Goldstein, 1997; Ni et al., 2001; Marambaud et al., 2003). In the case of Notch for instance, which controls cell fate selection throughout development, very small amounts of its intracellular domain (Notch-ICD), almost undetectable *in vivo*, have a strong biological effect in the nucleus (Schroeter et al., 1998). The γ-ICD might

very well exert signaling mechanisms in the nucleus in a similar manner. Indeed, the level of γ-ICD is also virtually undetectable in the nucleus unless proteasome inhibitors are added. Nuclear translocation of the γ-ICD and gene transactivation have been demonstrated (Hambsch et al., 2005). Thus, a significant part of my work concentrated on the signaling function of this domain.

4.2 γ-Pcdhs and brain complexity: the search for interaction partners

Considering brain complexity, one of the most interesting questions regards the intricate interconnections between myriads of neurons and how they are generated, especially in regions related to higher brain functions such as the neocortex. Thus, in our search for γ-Pcdhs interaction partners we utilized immunoprecipitation of extracts from mouse forebrain for mass spectrometry (MS). We chose, newborn (P0) and young adults (P42) for our analysis, since we assumed that γ-Pcdhs might be involved in the development of neuronal networks, and that different interacting complexes may interact with them during different developmental stages. While synaptogenesis peaks in the first two weeks after birth to establish the basic brain circuitry, at P42, it is mainly associated with plasticity and learning functions (Stern et al., 2001). Unexpectedly, we found similar proteins in both age groups, a result suggesting similar signaling functions during early and late postnatal development.

Recently, another search for γ-Pcdhs interacting proteins has been reported (Chen et al., 2008). These authors performed a yeast two hybrid screen from an adult mouse brain cDNA library and were able to identify two tyrosine kinases: PYK2 and FAK as γ-Pcdh interactors. They showed that PYK2 activity is abnormally up-regulated in γ-Pcdh deficient neurons and that overexpression of PYK2 induces apoptosis in chicken spinal cord. Thus, they claim that negative regulation of PYK2 activity by Pcdhs (α- and γ-Pcdhs) contributes to the survival of subsets of spinal neurons. The connection made between γ-Pcdh signaling and apoptosis is, however, not entirely new as this has already been shown in the spinal cord of knock-out mice (Weiner et al., 2005).

Interestingly, we detected neither PYK2, nor FAK by MS. There are several possible reasons for this, probably originating from the different methods employed. Chen et al. (2008) preformed a yeast two-hybrid assay, followed by transfection of the interactors and verification of their association by immunoprecipitation in HEK293T cell lysates, and further functional verification in chicken spinal cord *in vivo*. The yeast two-hybrid system, for several reasons, might have given different results when compared to our method. First, it utilizes peptides and not native proteins to fish interacting proteins. Second, the yeast two-hybrid system utilizes chimeric proteins, a fusion between a transcription factor and a fragment of the investigated protein (bait). The protein fusion might change the native conformation of the bait and/or prey (interacting protein) and might consequently alter binding properties. Third, the use of yeast as hosts may result in misfolding, as well as inappropriate post-translational modifications of the studied proteins. Last, some proteins might be toxic for yeast and therefore not be represented in the library (Van Criekinge and Beyaert, 1999). Another possible source for variation is the origin of the material with which we, and Chen et al. (2008) worked: protein lysates and a cDNA clones from library, respectively. Proteins whose endogenous levels are low might not be detected in our approach, and proteins which associate with γ-Pcdhs as a part of a complex might not be detected in the yeast two-hybrid approach. In our study we chose immunoprecipitation from brain lysates, analyzed by MS, to identify proteins interacting with γ-Pcdhs. This method is very sensitive, accurate and allows the use of the original mouse model system (Hale et al., 2000).

In conclusion, we show that MS analysis yields other protein partners, which might unravel a role of γ-Pcdhs in the formation of brain complexity. Our results discussed herein support this hypothesis.

In the following we discuss the nature of γ-Pcdh interacting proteins identified and verified by us, considering first the KH domain containing, RNA binding, signal transduction associated proteins, Sam68 and SLM-2.

4.3 Sam68 and SLM-2: γ-Pcdhs interacting proteins reveal possible functions of γ-Pcdhs

Sam68 was originally identified as the major target for Src phosphorylation during mitosis (hence the name: Src-associated in mitosis 68 kDa protein) and contains several Src Homology domains (SH2 and SH3), as well as a classic KH2 RNA binding domain. Its exact function is not clear (Rajan et al., 2008). SLM-2 (Sam68-like mammalian protein 2) is a close homologue of Sam68, which probably participates in similar pathways (Di Fruscio et al., 1999).

A variety of possible biological roles have been proposed for Sam68 including mitosis and cell cycle regulation, signal transduction, tumor suppression, regulation of alternative splice site selection and even retro-viral transport (Lukong and Richard, 2003). Interestingly, Sam68 and SLM-2 (as well as SLM-1) have been shown to localize in Sam68/SLM nuclear bodies, called SNBs in cancer cell lines (Chen et al., 1999).

Sam68 is predominantly nuclear but is phosphorylated in the cytoplasm by both Src and ERK, and acts as a transcriptional regulator. This is of interest as Both the Src and ERK proteins that interact with Sam68 have been implicated in signal transduction pathways involved in neuronal properties such as synaptic plasticity and long-term memory. In fact, Src is believed to upregulate the activity of NMDA receptors, critical molecules in synaptic plasticity (Kalia et al., 2004; Sweatt, 2004). These proteins, participating in major signal transduction pathways related to the cell cycle, also serve as regulators of long term plasticity and memory in neurons. For example, inhibition of ERK phosphorylation inhibits the formation of long-term taste aversion memory (Berman et al., 1998). A function of these pathways in neurons other than their “classic” role in other cell types might be possible since, unlike other cell types, neurons very rarely undergo cell division (Zhao et al., 2008).

In this regard, it is important to review the known facts about the function of Sam68 in neurons. Sam68 has been shown to bind different sets of RNAs in different cell types (Grange et al., 2009), and has been shown to be expressed in the somatodendritic compartment of neurons, where it associates with dendritically localized mRNAs, probably via its KH2 domain. Very recently, Sam68 was immunoprecipitated from

cultured hippocampal neurons and several mRNAs bound to it were identified using microarray screening (including the activity-responsive mRNA coding for translation elongation factor eEF1A; Grange et al. (2009). Another important finding from this study was an interaction between Sam68 and the NMDA receptor. This could potentially provide an indirect link between γ-Pcdhs and synaptic plasticity. Furthermore, Sam68 has been implicated in the regulation of a set of alternatively spliced exons during neurogenesis. Differentiation of primary neuronal progenitor cells from embryonic mouse neocortex was shown to be promoted by overexpression of Sam68, and suppressed by its loss (Rajan et al., 2008; Chawla et al., 2009). We propose several mechanisms through which the interaction between Sam68 and γ-Pcdhs may take place in neurons.

First, Sam68 may regulate cell-cycle progression downstream to γ-Pcdh signalling, similar to spinal cord neurons (though likely not via PYK2). Second, Sam68 may propagate a proliferation signal to subsets of neurons during neurogenesis, and thus help in the formation of functional neuronal circuits. Since the association of Sam68 with cell-cycle regulation is currently unclear (Rajan et al., 2008), both options are still a matter for speculation. Third, it is tempting to speculate that Sam68 operates in the complex alternative splicing of γ-Pcdhs. Thus Sam68 together with the γ-ICD might affect a cell's 'signature' - its differential display of γ-Pcdhs isoforms on the cell surface. A fourth possibility, inherently different from the functions described up to date for the γ-Pcdhs is that Sam68 functions downstream of the γ-Pcdhs in forebrain neurons via the Erk and Src pathways to activate gene regulation affecting the long term shaping of synapses.

4.4 Other γ-Pcdhs interacting proteins

Another bona-fide γ-Pcdhs interaction partner is the G-coupled, inward rectifying K^+ channel, Kir3.1. This is a member of a large family of ion channel proteins which, as their name implies, mediated inward potassium currents via a G-protein coupled receptor. It is very difficult to assign a specific function to this protein as this family is involved in the regulation of various morphogenetic events, such as the proliferation, differentiation and survival of neurons and glia cells (Neusch et al., 2003). The absence of other proteins

involved with Kir-related pathways by MS analysis, makes is difficult to speculate on the physiological implications of the Kir3.1-γ-Pcdhs interaction.

Our analysis also revealed a number of γ-Pcdhs interacting proteins, which we did not yet verify by immunoprecipitation, but that may have significance for the function of γ-Pcdhs. For example, our list of interactors includes a large group of proteins that are involved in RNA metabolism. SART3 (squamous cell carcinoma antigen recognized by T cells 3), for example, is an RNA binding protein about which little is known, except that it is thought to regulate RNA splicing in the nucleus (Harada et al., 2000). Likewise, LSm proteins, including LSm3 and LSm8 (which were detected in our analysis) have been shown to interact with the spliceosome, including with the U6 snRNA, and SART3 (also known as p110; (Licht et al., 2008). In light of the complex alternative splicing which underlies the diversity of Pcdhs, and given that the γ-ICD is able to upregulate the expression of the γ-Pcdh transcripts (Hambsch et al., 2005), an interesting possibility is that the γ-ICD helps to regulate its own splicing via binding to these proteins (LSm and SART3). In this respect, we also detected several heterogeneous nuclear ribonucleoproteins that contain RRM motifs, known to interact with mRNA and to regulate a variety of processes, including splicing (NCBI conserved domain database, domain cd00590:RRM). Another possiblity, of course, is that splicing regulation affects RNAs, which regulate different developmental aspects of neuronal connectivity. These effects would not necessarily be mutually exclusive.

Other proteins which we have detected as γ-Pcdhs interactors but are not verified yet may also have relevance for the biological function of γ-Pcdhs. For example, STUB1 (STIP1 homology and U-box-containing protein 1, also known as CHIP which has an E3-ubiquitin ligase activity and targets misfolded chaperone substrates towards proteasomal degradation (Wang and DeFranco, 2005), could potentially also regulate γ-ICD levels in a similar mechanism. Indeed, for both α- and γ-ICD, inhibition of the proteasomal pathway was shown to cause their accumulation (Hambsch et al., 2005; Bonn et al., 2007). Interestingly, a large yeast two-hybrid screen identified an interaction between STUB1 and Sam68 (Stelzl et al., 2005). STUB1 could be involved in proteasomal degradation of Sam68. Further research is needed to clarify the pertinent interactions in forebrain neurons.

How may we be sure of the validity of the interaction proteins that we did not yet verify? One finding that supports our results is the pull-down of several α- and γ-Pcdh isoforms (Bonn et al., 2007). A control that was not done in my work, though, was immunoprecipitation from γ-Pcdh knock-out mice. This was because knock-out mice die within a few hours after birth, making it necessary to process the brains immediately as they are born. We hope to address these issues with further experiments in the future.

4.5 Current models for γ-Pcdhs research

To date, most research has focused on genetic models, in which γ-Pcdhs were deleted globally or conditionally (Wang et al., 2002b; Hambsch et al., 2005; Weiner et al., 2005; Lefebvre et al., 2008; Prasad et al., 2008). As the deletion of γ-Pcdhs resulted in perinatal lethality, it was impossible to assess their function in the post-natal cortex. Unfortunately, γ-Pcdhs heterozygous mice do not contribute much information. Though the remaining level of γ-Pcdh proteins in heterozygotes is about 25% of the wild-type (Hambsch et al., 2005), only mild phenotypic effects are seen (a behavioral effect on the transfer of categorized information was detected in the heterozygous mice, our own unpublished data). Furthermore, there are three Pcdh cluster, the α-, β-, and γ-Pcdhs. The α- and γ-Pcdhs appear to display very similar extracellular properties, and they show similar proteolytic processing and nuclear transport of their ICD (Bonn et al., 2007). The ICDs of α- and γ-Pcdhs, however, are not homologus, which makes it very difficult to address the question of functional redundancy.

We were interested in studying the possible effects of the γ-Pcdhs and especially of the γ-ICD on synaptogenesis and synaptic plasticity. To study these functions we may have to "push" the system by overexpression and/or mutagenesis of the proteins involved in intracellular signaling. For *in vivo* studies of signaling pathways, we needed to develope a system which allows overexpression of the γ-ICD, the putative signaling molecule, by means of neonatal viral injection in forbrain. This, in combination with our identified γ-Pcdhs binding partners might be a promising course of action for the elucidation of the signal transduction pathways through which γ-Pcdhs exert their biological function.

The amount of γ-Pcdh expression is highest in neonates (Frank et al., 2005), a trait which is achieved with our viral expression system. Furthermore, this time window is also critical for the establishments of synapses, and thus synaptic plasticity (Hooks and Chen, 2007; Maffei and Turrigiano, 2008).

4.6 Expression of transgenes by virus-mediated gene transfer into neonatal mouse brains

There are several methods to overexpress exogenous gene products in the brain. We dismissed classic transgenics for reasons of the time and labor involved, especially since we wanted a versatile and rapid system in which we could potentially express different candidate binding partners of the γ-Pcdhs, as well as mutants thereof (e.g. in potential interaction domains). Only viral gene delivery into newborns would fulfill all these requirements.

Virally mediated gene transfer is a valuable tool for the infection of defined brain regions with high spatial and temporal resolution. It allows us to reliably infect neuronal cell populations in neonatal mice brain with high a degree of precision. Notably, the use of cell type specific promoters allows even more selective targeting of desired neuronal populations. For example, the human synapsin core promoter/enhancer element that we used, is relatively short (300 bp), and permits efficient transduction of neurons.

The disproportionately large size of the ventricles in the brains of newborn mice allows the injection of a relatively large volume of virus containing solution and thus an efficient systemic infection. We have shown that results are reliable and reproducible, expression starts at a distinct time point, depending on the promoter as early as 24 hours after injection, and in selective neuronal populations, and may last throughout life. Brain damage is negligible as we could not detect any tissue damage or necrosis at the site of injection even two weeks after injection of the purified viruses.

Our technique is especially useful in combination with preexisting transgenic mouse lines, specifically those with conditional genes surrounded by LoxP elements ("floxed alleles"). For example, in the present work, heterozygous *Rosa26*^{2lox} indicator mice were infected after birth with a virus expressing Cre-recombinase in the region and cell type of

interest, or upon ventricular injection, in the entire neocortex. The apparent success and efficiency of this method should bypass laborious and time consuming matings with deleter mouse-lines expressing Cre-recombinase. Most notably, embryonic expression, often a problem with transgenics (and obviously a problem for γ-Pcdhs), due to onset of expression during early development, can be avoided with this method. Furthermore, a reporter can be combined into this system: as described here, expression of the GFP reporter protein is detectable 24 hours after injection. Due to the relatively small molecular weight of the Cre-recombinase, and of the γ-ICD, even rAAVs which have a relatively small genome (about 6kb, Grimm et al., 1998), can be additionally equipped with a fluorescent marker protein. This would allow for fast and easy visual inspection of the targeted region, both in tissue slices and, with the advent of new microscopic techniques, in whole organ preparations or even '*in vivo*'.

4.7 Physiological phenotypes detected using neonatal overexpression of γ-ICD in forebrain; future prospects for γ-Pcdhs research

Using our viral transduction system in neonates, we attempted first to overexpress the entire γ-Pcdh A1. Unfortunately, our results proved unsatisfactory; only a low level of expression was detected. This was probably due to the large size of the coding sequence and limits in packaging size of rAAV, as we successfully overexpressed the shorter γ-ICD fragment, much above endogenous levels. As a first step we measured physiological effects after γ-ICD overexpression in pyramidal neurons by recording synaptic currents. Preliminary results demonstrate that miniature inhibitory post synaptic currents (mIPSCs) were greatly increased in amplitude in γ-ICD infected neurons. This novel finding is specific for the inhibitory post-synaptic compartment, since excitatory miniature synaptic currents (mEPSCs) in the very same cells were not affected. This provides a tool for further investigation of the functions of γ-Pcdhs and their interaction partners. Our results afford a phenotypic "handle" on which to base future research.

Previous studies on the effects of γ-Pcdhs on synaptic transmission have yielded controversial results and were, in any event limited to interneurons (in the spinal cord and

in the retina, (Weiner et al., 2005; Lefebvre et al., 2008). However, no physiological results have been reported to date for pyramidal neurons in the cortex.

Our data revealed a variety of novel interaction partners for γ-Pcdhs, at least one of which, Sam68, actually binds dendritic mRNAs (Grange et al., 2009). Unfortunately, very little work has been performed with Sam68 in primary neurons or *in vivo*, and most of the literature reports on its role in cancer. One of our future challenges would be to examine the way the various putative γ-Pcdhs interaction partners interact with the inhibitory post-synapse, by expression of these proteins and mutants thereof, and measuring its effects on mIPSCs. Another important question, which may be raised, is does the overexpression of the γ-ICD act to inhibit the function of the endogenous γ-Pcdhs by sequestering endogenous binding partners, or does it act as a constitutively active γ-Pcdh? We hope to answer this question by comparing the phenotype of targeted γ-Pcdh deletion in the conditional *γ-Pcdh*^{2lox} mouse line (Hambsch et al., 2005) by means of neonatal Cre recombinase expressing virus injection, together with that of the γ-ICD overexpression.

In conclusion, using biochemical methods, and a specialized viral vector delivery system, we present previously unknown interaction candidates for the γ-Pcdhs, as well as novel physiological findings. This study details ongoing work aimed at deciphering the function and mechanism of γ-Pcdhs intracellular signaling in the brain. We hope to shed light on the signal transduction pathways which connect the formation of brain circuitry with the genetic programming in the brain.

5. Abbreviations

CB:	Cerebellum
CNS:	Central Nervous System
DDW:	Double Distilled Water
EC:	Extracellular Cadherin
ERK:	Extracellular Regulated Kinase
FC:	Frontal Cortex
GFP:	Green Fluorescent Protein
HPc:	Hippocampus
ICD:	Intracellular Constant Domain
IP:	Immunoprecipitation
IRES:	Internal Ribosomal Entry Site
KO:	Knock-Out
mE/IPSCs:	Miniature Excitatory/Inhibitory Post-Synaptic Currents
MS:	Mass Spectrometry
NLS:	Nuclear Localization Signal
NMDA:	N-Methyl D-Aspartic Acid
OB:	Olfactory Bulb
Pcdh:	Protocadherins
PS-IP:	Presenilin Dependent Intramembrane Proteolysis
rAAV:	Recombinant Adeno-Associated Virus
Sam68:	Src Associated in Mitosis, 68 kDa Protein
SLM-2:	Sam68 Like Mammalian Protein 2
SNPs:	Single Nucleotide Polymorphism
Sup:	Supernatant
TTX:	Tetrodotoxin
Ven:	Ventricles
WB:	Western Blot
WT:	Wild-Type
X-linked:	Cross linked

6. Acknowledgements

I wish to thank the people who helped me throughout the course of my Ph.D. and with the writing of this thesis.

Prof. Peter H. Seeburg, for giving me the chance, and for your continuous support.
Dr. Martin Schwarz, who was with me hands on throughout these three years. I am deeply grateful, words cannot express…
My examiners, Profs. Michael Brunner, Stephan Frings, and Dr. Matthias Klugmann, for being on my committee.
Florian Freundenberg, for being my best friend and colleague.
Natalie Landeck, for being the sweet person that you are, for your endless help, and for finishing my sentences…
All my friends in the lab, Sophie, Melanie, Evgeny, Sascha, Pawel, Valery, and all the many others who helped me and laughed with me.
All the wonderful technicians in the department, Judith, Sabine, Annette, and Horst.
My family, Ima, Aba, Oneg, and Aner. For lifting my spirit, and for all the love throughout the years. To my father for constructive scientific discussions.
Shaiy and Nurit, for always being there.
My beloved Marion, who gave us a feeling of a family here in Germany, and the peace of mind to go back to work after childbirth. You're one of a kind.
My husband, Yair, you are the air that I breath. For being my motivation, for giving me endless support, and for always urging me on.
My daughter, Eden (Pilpel and Pilpel, 2008), for being the love and light of my life. The best part of the day is coming home and seeing your smile.

7. References

Ahimou F, Mok LP, Bardot B, Wesley C (2004) The adhesion force of Notch with Delta and the rate of Notch signaling. J Cell Biol 167:1217-1229.

Alagramam KN, Yuan H, Kuehn MH, Murcia CL, Wayne S, Srisailpathy CR, Lowry RB, Knaus R, Van Laer L, Bernier FP, Schwartz S, Lee C, Morton CC, Mullins RF, Ramesh A, Van Camp G, Hageman GS, Woychik RP, Smith RJ (2001) Mutations in the novel protocadherin PCDH15 cause Usher syndrome type 1F. Hum Mol Genet 10:1709-1718.

Berman DE, Hazvi S, Rosenblum K, Seger R, Dudai Y (1998) Specific and differential activation of mitogen-activated protein kinase cascades by unfamiliar taste in the insular cortex of the behaving rat. J Neurosci 18:10037-10044.

Bonn S, Seeburg PH, Schwarz MK (2007) Combinatorial expression of alpha- and gamma-protocadherins alters their presenilin-dependent processing. Mol Cell Biol 27:4121-4132.

Broekman ML, Comer LA, Hyman BT, Sena-Esteves M (2006) Adeno-associated virus vectors serotyped with AAV8 capsid are more efficient than AAV-1 or -2 serotypes for widespread gene delivery to the neonatal mouse brain. Neuroscience 138:

Brown MS, Goldstein JL (1997) The SREBP pathway: regulation of cholesterol metabolism by proteolysis of a membrane-bound transcription factor. Cell 89:331-340.

Burger C, Nash K, Mandel RJ (2005) Recombinant adeno-associated viral vectors in the nervous system. Hum Gene Ther 16:781-791.

Capecchi MR (1989a) The new mouse genetics: altering the genome by gene targeting. Trends Genet 5:70-76.

Capecchi MR (1989b) Altering the genome by homologous recombination. Science 244:1288-1292.

Chawla G, Lin CH, Han A, Shiue L, Ares M, Jr., Black DL (2009) Sam68 regulates a set of alternatively spliced exons during neurogenesis. Mol Cell Biol 29:201-213.

Chen J, Lu Y, Meng S, Han MH, Lin C, Wang X (2008) Alpha- and Gamma-protocadherins negatively regulate PYK2. J Biol Chem.

Chen T, Boisvert FM, Bazett-Jones DP, Richard S (1999) A role for the GSG domain in localizing Sam68 to novel nuclear structures in cancer cell lines. Mol Biol Cell 10:3015-3033.

Di Fruscio M, Chen T, Richard S (1999) Characterization of Sam68-like mammalian proteins SLM-1 and SLM-2: SLM-1 is a Src substrate during mitosis. Proc Natl Acad Sci U S A 96:2710-2715.

Esumi S, Kakazu N, Taguchi Y, Hirayama T, Sasaki A, Hirabayashi T, Koide T, Kitsukawa T, Hamada S, Yagi T (2005) Monoallelic yet combinatorial expression of variable exons of the protocadherin-alpha gene cluster in single neurons. Nat Genet 37:171-176.

Frank M, Ebert M, Shan W, Phillips GR, Arndt K, Colman DR, Kemler R (2005) Differential expression of individual gamma-protocadherins during mouse brain development. Mol Cell Neurosci 29:603-616.

Grange J, Belly A, Dupas S, Trembleau A, Sadoul R, Goldberg Y (2009) Specific interaction between Sam68 and neuronal mRNAs: implication for the activity-dependent biosynthesis of elongation factor eEF1A. J Neurosci Res 87:12-25.

Grimm D, Kern A, Rittner K, Kleinschmidt JA (1998) Novel tools for production and purification of recombinant adenoassociated virus vectors. Hum Gene Ther 9:2745-2760.

Haas IG, Frank M, Veron N, Kemler R (2005) Presenilin-dependent processing and nuclear function of gamma-protocadherins. J Biol Chem 280:9313-9319.

Hale JE, Butler JP, Knierman MD, Becker GW (2000) Increased sensitivity of tryptic peptide detection by MALDI-TOF mass spectrometry is achieved by conversion of lysine to homoarginine. Anal Biochem 287:110-117.

Hambsch B, Grinevich V, Seeburg PH, Schwarz MK (2005) {gamma}-Protocadherins, presenilin-mediated release of C-terminal fragment promotes locus expression. J Biol Chem 280:15888-15897.

Harada K, Yamada A, Mine T, Kawagoe N, Takasu H, Itoh K (2000) Mouse homologue of the human SART3 gene encoding tumor-rejection antigen. Jpn J Cancer Res 91:239-247.

Hartmann D, de Strooper B, Serneels L, Craessaerts K, Herreman A, Annaert W, Umans L, Lubke T, Lena Illert A, von Figura K, Saftig P (2002) The disintegrin/metalloprotease ADAM 10 is essential for Notch signalling but not for alpha-secretase activity in fibroblasts. Hum Mol Genet 11:2615-2624.

Hirayama T, Sugino H, Yagi T (2001) Somatic mutations of synaptic cadherin (CNR family) transcripts in the nervous system. Genes Cells 6:151-164.

Hooks BM, Chen C (2007) Critical periods in the visual system: changing views for a model of experience-dependent plasticity. Neuron 56:312-326.

Kalia LV, Gingrich JR, Salter MW (2004) Src in synaptic transmission and plasticity. Oncogene 23:8007-8016.

Kandel ER, Schwarz JH, Jessel TM (2000) Principles of Neural Science, 4th Edition.

Kaneko R, Kato H, Kawamura Y, Esumi S, Hirayama T, Hirabayashi T, Yagi T (2006) Allelic gene regulation of Pcdh-alpha and Pcdh-gamma clusters involving both monoallelic and biallelic expression in single Purkinje cells. J Biol Chem 281:30551-30560.

Knudson CM, Tung KS, Tourtellotte WG, Brown GA, Korsmeyer SJ (1995) Bax-deficient mice with lymphoid hyperplasia and male germ cell death. Science 270:96-99.

Kohmura N, Senzaki K, Hamada S, Kai N, Yasuda R, Watanabe M, Ishii H, Yasuda M, Mishina M, Yagi T (1998) Diversity revealed by a novel family of cadherins expressed in neurons at a synaptic complex. Neuron 20:1137-1151.

Kugler S, Lingor P, Scholl U, Zolotukhin S, Bahr M (2003) Differential transgene expression in brain cells in vivo and in vitro from AAV-2 vectors with small transcriptional control units. Virology 311:89-95.

Lammich S, Kojro E, Postina R, Gilbert S, Pfeiffer R, Jasionowski M, Haass C, Fahrenholz F (1999) Constitutive and regulated alpha-secretase cleavage of Alzheimer's amyloid precursor protein by a disintegrin metalloprotease. Proc Natl Acad Sci U S A 96:3922-3927.

Lefebvre JL, Zhang Y, Meister M, Wang X, Sanes JR (2008) {gamma}-Protocadherins regulate neuronal survival but are dispensable for circuit formation in retina. Development 135:4141-4151.

Licht K, Medenbach J, Luhrmann R, Kambach C, Bindereif A (2008) 3'-cyclic phosphorylation of U6 snRNA leads to recruitment of recycling factor p110 through LSm proteins. Rna 14:1532-1538.

Ling Y, Morgan K, Kalsheker N (2003) Amyloid precursor protein (APP) and the biology of proteolytic processing: relevance to Alzheimer's disease. Int J Biochem Cell Biol 35:1505-1535.

Lukong KE, Richard S (2003) Sam68, the KH domain-containing superSTAR. Biochim Biophys Acta 1653:73-86.

Maffei A, Turrigiano G (2008) The age of plasticity: developmental regulation of synaptic plasticity in neocortical microcircuits. Prog Brain Res 169:211-223.

Marambaud P, Wen PH, Dutt A, Shioi J, Takashima A, Siman R, Robakis NK (2003) A CBP binding transcriptional repressor produced by the PS1/epsilon-cleavage of N-cadherin is inhibited by PS1 FAD mutations. Cell 114:635-645.

Maretzky T, Reiss K, Ludwig A, Buchholz J, Scholz F, Proksch E, de Strooper B, Hartmann D, Saftig P (2005) ADAM10 mediates E-cadherin shedding and regulates epithelial cell-cell adhesion, migration, and beta-catenin translocation. Proc Natl Acad Sci U S A 102:9182-9187.

Marrs JA, Nelson WJ (1996) Cadherin cell adhesion molecules in differentiation and embryogenesis. Int Rev Cytol 165:159-205.

Miki R, Hattori K, Taguchi Y, Tada MN, Isosaka T, Hidaka Y, Hirabayashi T, Hashimoto R, Fukuzako H, Yagi T (2005) Identification and characterization of coding single-nucleotide polymorphisms within human protocadherin-alpha and -beta gene clusters. Gene 349:1-14.

Morishita H, Yagi T (2007) Protocadherin family: diversity, structure, and function. Curr Opin Cell Biol 19:584-592.

Morishita H, Umitsu M, Murata Y, Shibata N, Udaka K, Higuchi Y, Akutsu H, Yamaguchi T, Yagi T, Ikegami T (2006) Structure of the cadherin-related neuronal receptor/protocadherin-alpha first extracellular cadherin domain reveals diversity across cadherin families. J Biol Chem 281:33650-33663.

Mutoh T, Hamada S, Senzaki K, Murata Y, Yagi T (2004) Cadherin-related neuronal receptor 1 (CNR1) has cell adhesion activity with beta1 integrin mediated through the RGD site of CNR1. Exp Cell Res 294:494-508.

Neusch C, Weishaupt JH, Bahr M (2003) Kir channels in the CNS: emerging new roles and implications for neurological diseases. Cell Tissue Res 311:131-138.

Nguyen T, Sudhof TC (1997) Binding properties of neuroligin 1 and neurexin 1beta reveal function as heterophilic cell adhesion molecules. J Biol Chem 272:26032-26039.

Ni CY, Murphy MP, Golde TE, Carpenter G (2001) gamma -Secretase cleavage and nuclear localization of ErbB-4 receptor tyrosine kinase. Science 294:2179-2181.

Noonan JP, Grimwood J, Schmutz J, Dickson M, Myers RM (2004) Gene conversion and the evolution of protocadherin gene cluster diversity. Genome Res 14:354-366.

Noonan JP, Li J, Nguyen L, Caoile C, Dickson M, Grimwood J, Schmutz J, Feldman MW, Myers RM (2003) Extensive linkage disequilibrium, a common 16.7-kilobase deletion, and evidence of balancing selection in the human protocadherin alpha cluster. Am J Hum Genet 72:621-635.

Paxinos G, Watson CR, Emson PC (1980) AChE-stained horizontal sections of the rat brain in stereotaxic coordinates. J Neurosci Methods 3:129-149.

Phillips GR, Tanaka H, Frank M, Elste A, Fidler L, Benson DL, Colman DR (2003) Gamma-protocadherins are targeted to subsets of synapses and intracellular organelles in neurons. J Neurosci 23:5096-5104.

Phillips GR, Huang JK, Wang Y, Tanaka H, Shapiro L, Zhang W, Shan WS, Arndt K, Frank M, Gordon RE, Gawinowicz MA, Zhao Y, Colman DR (2001) The presynaptic particle web: ultrastructure, composition, dissolution, and reconstitution. Neuron 32:63-77.

Pilpel Y, Kolleker A, Berberich S, Ginger M, Frick A, Mientjes E, Oostra BA, Seeburg PH (2008) Synaptic ionotropic glutamate receptors and plasticity are developmentally altered in the CA1 field of FMR1 KO mice. J Physiol.

Prasad T, Wang X, Gray PA, Weiner JA (2008) A differential developmental pattern of spinal interneuron apoptosis during synaptogenesis: insights from genetic

analyses of the protocadherin-{gamma} gene cluster. Development 135:4153-4164.

Rajan P, Gaughan L, Dalgliesh C, El-Sherif A, Robson CN, Leung HY, Elliott DJ (2008) Regulation of gene expression by the RNA-binding protein Sam68 in cancer. Biochem Soc Trans 36:505-507.

Redies C, Vanhalst K, Roy F (2005) delta-Protocadherins: unique structures and functions. Cell Mol Life Sci 62:2840-2852.

Reiss K, Maretzky T, Haas IG, Schulte M, Ludwig A, Frank M, Saftig P (2006) Regulated ADAM10-dependent ectodomain shedding of gamma-protocadherin C3 modulates cell-cell adhesion. J Biol Chem 281:21735-21744.

Sambrook J, Gething MJ (1989) Protein structure. Chaperones, paperones. Nature 342:224-225.

Sano K, Tanihara H, Heimark RL, Obata S, Davidson M, St John T, Taketani S, Suzuki S (1993) Protocadherins: a large family of cadherin-related molecules in central nervous system. Embo J 12:2249-2256.

Schmucker D, Flanagan JG (2004) Generation of recognition diversity in the nervous system. Neuron 44:219-222.

Schroeter EH, Kisslinger JA, Kopan R (1998) Notch-1 signalling requires ligand-induced proteolytic release of intracellular domain. Nature 393:382-386.

Sela-Donenfeld D, Wilkinson DG (2005) Eph receptors: two ways to sharpen boundaries. Curr Biol 15:R210-212.

Soriano P (1999) Generalized lacZ expression with the ROSA26 Cre reporter strain. Nat Genet 21:70-71.

Stelzl U, Worm U, Lalowski M, Haenig C, Brembeck FH, Goehler H, Stroedicke M, Zenkner M, Schoenherr A, Koeppen S, Timm J, Mintzlaff S, Abraham C, Bock N, Kietzmann S, Goedde A, Toksoz E, Droege A, Krobitsch S, Korn B, Birchmeier W, Lehrach H, Wanker EE (2005) A human protein-protein interaction network: a resource for annotating the proteome. Cell 122:957-968.

Stern EA, Maravall M, Svoboda K (2001) Rapid development and plasticity of layer 2/3 maps in rat barrel cortex in vivo. Neuron 31:305-315.

Sweatt JD (2004) Mitogen-activated protein kinases in synaptic plasticity and memory. Curr Opin Neurobiol 14:311-317.

Sweatt JD (2009) Experience-dependent epigenetic modifications in the central nervous system. Biol Psychiatry 65:191-197.

Takeichi M (1990) Cadherins: a molecular family important in selective cell-cell adhesion. Annu Rev Biochem 59:237-252.

Takeichi M (1991) Cadherin cell adhesion receptors as a morphogenetic regulator. Science 251:1451-1455.

Takeichi M (1995) Morphogenetic roles of classic cadherins. Curr Opin Cell Biol 7:619-627.

Takeichi M (2007) The cadherin superfamily in neuronal connections and interactions. Nat Rev Neurosci 8:11-20.

Tasic B, Nabholz CE, Baldwin KK, Kim Y, Rueckert EH, Ribich SA, Cramer P, Wu Q, Axel R, Maniatis T (2002) Promoter choice determines splice site selection in protocadherin alpha and gamma pre-mRNA splicing. Mol Cell 10:21-33.

Tepass U, Truong K, Godt D, Ikura M, Peifer M (2000) Cadherins in embryonic and neural morphogenesis. Nat Rev Mol Cell Biol 1:91-100.

Uemura T (1998) The cadherin superfamily at the synapse: more members, more missions. Cell 93:1095-1098.

Van Criekinge W, Beyaert R (1999) Yeast Two-Hybrid: State of the Art. Biol Proced Online 2:1-38.

Wang X, DeFranco DB (2005) Alternative effects of the ubiquitin-proteasome pathway on glucocorticoid receptor down-regulation and transactivation are mediated by CHIP, an E3 ligase. Mol Endocrinol 19:1474-1482.

Wang X, Su H, Bradley A (2002a) Molecular mechanisms governing Pcdh-gamma gene expression: evidence for a multiple promoter and cis-alternative splicing model. Genes Dev 16:1890-1905.

Wang X, Weiner JA, Levi S, Craig AM, Bradley A, Sanes JR (2002b) Gamma protocadherins are required for survival of spinal interneurons. Neuron 36:843-854.

Weidemann A, Konig G, Bunke D, Fischer P, Salbaum JM, Masters CL, Beyreuther K (1989) Identification, biogenesis, and localization of precursors of Alzheimer's disease A4 amyloid protein. Cell 57:115-126.

Weiner JA, Wang X, Tapia JC, Sanes JR (2005) Gamma protocadherins are required for synaptic development in the spinal cord. Proc Natl Acad Sci U S A 102:8-14.

Wu Q, Maniatis T (1999) A striking organization of a large family of human neural cadherin-like cell adhesion genes. Cell 97:779-790.

Wu Q, Zhang T, Cheng JF, Kim Y, Grimwood J, Schmutz J, Dickson M, Noonan JP, Zhang MQ, Myers RM, Maniatis T (2001) Comparative DNA sequence analysis of mouse and human protocadherin gene clusters. Genome Res 11:389-404.

Yagi T (2003) Diversity of the cadherin-related neuronal receptor/protocadherin family and possible DNA rearrangement in the brain. Genes Cells 8:1-8.

Zhao C, Deng W, Gage FH (2008) Mechanisms and functional implications of adult neurogenesis. Cell 132:645-660.

Zhu P, Aller MI, Baron U, Cambridge S, Bausen M, Herb J, Sawinski J, Cetin A, Osten P, Nelson ML, Kugler S, Seeburg PH, Sprengel R, Hasan MT (2007) Silencing and un-silencing of tetracycline-controlled genes in neurons. PLoS ONE 2:e533.